

# The potential role of organics in new particle formation and initial growth in the remote tropical upper troposphere

Agnieszka Kupc<sup>1,2</sup>, Christina J. Williamson<sup>1,3</sup>, Anna L. Hodshire<sup>4</sup>, Jan Kazil<sup>1,3</sup>, Eric Ray<sup>1,3</sup>, T. Paul, Bui<sup>5</sup>, Maximilian Dollner<sup>2</sup>, Karl D. Froyd<sup>1,3</sup>, Kathryn McKain<sup>3,6</sup>, Andrew Rollins<sup>1</sup>, Gregory P. Schill<sup>1,3</sup>, Alexander Thames<sup>7</sup>, Bernadett B. Weinzierl<sup>2</sup>, Jeffrey R. Pierce<sup>4</sup> and Charles A. Brock<sup>1</sup>

<sup>1</sup>Chemical Sciences Laboratory, National Oceanic and Atmospheric Administration, Boulder, CO 80305, U.S.A

<sup>2</sup>Faculty of Physics, Aerosol Physics and Environmental Physics, University of Vienna, 1090 Vienna, Austria

<sup>3</sup>Cooperative Institute for Research in Environmental Sciences, University of Colorado, Boulder, CO 80309, U.S.A.

<sup>4</sup>Department of Atmospheric Science, Colorado State University, Fort Collins, CO 80523, USA

<sup>5</sup>Earth Science Division, NASA Ames Research Center, Moffett Field, California, USA

<sup>6</sup>Global Monitoring Laboratory, National Oceanic and Atmospheric Administration, Boulder, CO, 80305, USA

<sup>7</sup>Department of Meteorology and Atmospheric Science, Pennsylvania State University, University Park, PA, USA

*Correspondence to:* Agnieszka Kupc ([agnieszka.kupc@univie.ac.at](mailto:agnieszka.kupc@univie.ac.at))

## Abstract.

Global observations and model studies indicate that new particle formation (NPF) in the upper troposphere (UT) and subsequent particles supply 40-60 % of cloud condensation nuclei (CCN) in the lower troposphere, thus affecting the Earth's radiative budget. There are several plausible nucleation mechanisms and precursor species in this atmospheric region, which, in the absence of observational constraints, lead to uncertainties in modeled aerosols. In particular, the type of nucleation mechanism and concentrations of nucleation precursors, in part, determine the spatial distribution of new particles and resulting spatial distribution of CCN from this source. Although substantial advances in understanding NPF have been made in recent years, NPF processes in the UT in pristine marine regions are still poorly understood and are inadequately represented in global models.

Here, we evaluate commonly used and state-of-the-art NPF schemes in a Lagrangian box model to assess which schemes and precursor concentrations best reproduce detailed in situ observations. Using measurements of aerosol size distributions ( $0.003 < D_p < 4.8 \mu\text{m}$ ) in the remote marine troposphere between ~0.18 and 13 km altitude obtained during the NASA Atmospheric Tomography (ATom) mission, we show that high concentrations of newly formed particles in the tropical UT over both the Atlantic and Pacific oceans are associated with outflow regions of deep convective clouds. We focus analysis on observations over the remote Pacific Ocean, which is a region less perturbed by continental emissions than the Atlantic. Comparing aerosol size distribution measurements over the remote Pacific with box-model simulations for 32 cases shows that none of the NPF schemes most commonly used in global models, including binary nucleation of sulfuric acid and water

33 (neutral and ion-assisted) and ternary involving sulfuric acid, water, and ammonia, are consistent with observations, regardless  
34 of precursor concentrations. Through sensitivity studies, we find that the nucleation scheme among those tested that is able to  
35 explain most consistently (21 of 32 cases) the observed size distributions is that of Riccobono et al. (2014), which involves  
36 both organic species and sulfuric acid. The method of Dunne et al. (2016), involving charged sulfuric acid-water-ammonia  
37 nucleation, when coupled with organic growth of the nucleated particles, was most consistent with the observations for 5 of  
38 32 cases. Similarly, the neutral sulfuric acid-water-ammonia method of Napari (2002), when scaled with a tuning factor and  
39 with organic growth added was most consistent for 6 of 32 cases. We find that to best reproduce both nucleation and growth  
40 rates, the mixing ratios of gas-phase organic precursors generally need to be at least twice that of SO<sub>2</sub>, a proxy for dimethyl  
41 sulfide (DMS). Unfortunately, we have no information on the nature of oxidized organic species that participated in NPF in  
42 this region. Global models rarely include organic-driven nucleation and growth pathways in UT conditions where globally  
43 significant NPF takes place, which may result in poor estimates of NPF and CCN abundance and contribute to uncertainties  
44 in aerosol-cloud-radiation effects. Furthermore, our results indicate the organic aerosol precursor vapors may be important in  
45 the tropical UT above marine regions, a finding that should guide future observational efforts.

## 46 **1 Introduction**

47 The majority of particles found in the atmosphere are formed through gas-to-particle conversion (i.e. nucleation) from  
48 clustering of low-volatility vapors (Gordon et al., 2017; Pierce, 2017). While the formation of these molecular clusters appears  
49 to take place almost everywhere and at all times in the atmosphere (Kerminen et al., 2018), the formation of thermodynamically  
50 stable aerosol particles with diameters ( $D_p$ )  $\geq 1.5$  nm requires favorable conditions in terms of temperature, availability of  
51 condensable vapors, and the background of pre-existing bigger particles that compete for condensing vapors, and so may not  
52 occur in every atmospheric environment (Kulmala et al., 2014). Most of these newly formed particles are lost by coagulation  
53 with larger particles, and do not contribute to particle number (Westervelt et al., 2014). A subset of the nucleated particles  
54 grows by condensation to become larger particles with reduced Brownian motion, and hence lower coagulation loss rates  
55 (e.g., Pierce and Adams, 2007). Particles with  $D_p \gtrsim 50$  nm can serve as CCN at supersaturations found in typical marine  
56 cumulus and stratocumulus clouds (Quinn et al., 2008), increasing droplet number concentrations and cloud albedo, and thus  
57 indirectly affecting the Earth's radiative budget (Twomey, 1974; IPCC, 2013).

58 The tropical UT is known to be a major source region of new particles (e.g. Clarke, 1993; Brock et al., 1995; Clarke  
59 and Kapustin, 2002; Weigel et al., 2011; Williamson et al., 2019). This strong aerosol production is believed to be linked with  
60 frequent deep convection in this region. The mechanism proposed by Clarke (1992) involves the formation of new particles in  
61 the UT from convectively lifted and cloud-processed boundary layer air. At the conditions of cold temperatures, high photolytic  
62 fluxes, and low concentrations of pre-existing aerosol particles found in the outflow of deep convection at altitudes  $>8$  km,  
63 aerosol precursor gases that may survive convective transport and scavenging can oxidize and nucleate new particles which  
64 then grow to CCN sizes as they descend in the gradually subsiding air that compensates for the upward convection. Raes

65 (1995) used a box model to determine that observed concentrations of CCN in the remote marine boundary layer (MBL), and  
66 their temporal stability, could not be explained without a source of particles being entrained from the free troposphere (FT).  
67 Clarke et al. (2006) estimated that entrainment from the FT provides 35-80 % of the CCN flux into the MBL over latitudes  
68 between 40° S and 40° N with the rest coming from sea salt aerosol. More recently, Quinn et al. (2017) found that at ~0.5 %  
69 supersaturation, the accumulation mode aerosol, composed primarily of sulfate compounds rather than sea-spray particles,  
70 provides ~70 % of the CCN population throughout the MBL of the tropics and midlatitudes, and suggested that these particles  
71 originate from the FT.

72 Despite the climatic importance of NPF in the tropical UT, the chemical mechanisms are poorly understood (e.g.,  
73 English et al., 2011). This lack of understanding is driven by the fundamental complexity and variability of the atmosphere,  
74 the range of potential chemical species and mechanisms that could lead to NPF and subsequent growth of the newly formed  
75 particles to CCN, and the difficulty in obtaining observations of processes occurring in remote areas, at high altitudes, and  
76 over time scales ranging from minutes (NPF) to weeks (condensational growth during gradual descent). Together, these issues  
77 have made it difficult to validate NPF schemes used in global models and have hindered our ability to reduce uncertainty in  
78 aerosol-cloud-radiation interactions.

79 Williamson et al. (2019) showed that three of four global models examined in their study underestimated the  
80 magnitude of NPF in the tropical Pacific UT and all failed to accurately simulate the abundance of CCN-sized particles in the  
81 lower troposphere of the same region (the fourth model significantly overestimated aerosol loadings throughout the  
82 troposphere). None of these models used a NPF scheme involving organics, and the three models may lack sufficient precursor  
83 vapors for growth, in addition to other deficiencies. Previous model studies (e.g., Kazil et al., 2010; Yu et al., 2010; Zhang et  
84 al., 2010; Zhu et al., 2019) show that the choice of NPF mechanism can drive substantial changes in the predicted abundance  
85 and spatial distribution of particles. While Westervelt et al. (2014) suggested that the global-mean boundary layer CCN are  
86 not very sensitive to the number of particles formed in the UT due to the dampening effects of coagulation (i.e., more nucleation  
87 leads to faster coagulation losses), different choices of NPF mechanisms in models might alter the spatial and temporal  
88 pattern of NPF, and thus affect the spatial distribution and magnitude of CCN abundance. It is clear that accurate simulation  
89 of NPF and growth processes is essential to adequately represent particle size distributions and their spatial distribution in  
90 global models and improve predictions of aerosol-cloud-radiation effects (Hodshire et al., 2018; Williamson et al., 2019).

91 Field measurements have shown that sulfuric acid is a key component in atmospheric NPF in the continental boundary  
92 layer (e.g., Weber et al., 1997; Riipinen et al., 2007; Sihto et al., 2006). Several nucleation schemes involving sulfuric acid  
93 have been used in global models as a consequence. These include activation nucleation scheme that depends on sulfuric acid  
94 only (Kulmala et al., 2006), binary schemes that involve sulfuric acid and water to form new particles (e.g., Vehkamäki et al.,  
95 2002), or ternary schemes in which sulfuric acid, water and ammonia condense to form new particles (e.g., Napari et al. 2002).  
96 The activation nucleation scheme, however, is an empirical formulation tuned to mid-latitude continental boundary layer  
97 observations so it is appropriate to use only there. Binary NPF has been suggested to be favored in the remote tropical UT due  
98 to cold temperatures, high relative humidity (RH), and the availability of supersaturated sulfuric acid (Clarke, 1992; Brock et

99 al., 1995; Clarke and Kapustin, 2002). Ion-assisted nucleation of sulfuric acid and water clusters has been identified as a  
100 potential pathway for binary NPF (Kirkby et al., 2011; Lovejoy et al., 2004; Kazil and Lovejoy, 2007; Raes et al., 1997; Yu  
101 2010). Ions stabilize the molecular clusters so that nucleation can occur at warmer temperatures and lower nucleating-vapor  
102 concentrations (Yu, 2010).

103 Recent observations of the composition of molecular clusters present during NPF have highlighted the role that  
104 organics may play (Kulmala et al., 2013; Smith et al., 2004). Murphy et al. (2006) and Froyd et al. (2009) found that larger  
105 particles ( $D_p > 0.15 \mu\text{m}$ ) in the UT contained significant organic matter that was likely secondary, which suggests that  
106 condensable gas-phase organic compounds are present in the UT. Andreae et al. (2018) postulated that biogenic volatile organic  
107 compounds carried from the boundary layer to the UT by deep convection and oxidized to form condensable species over the  
108 Amazon are responsible for NPF observed in this continental UT region. Weigel et al. (2011) also suggested that organics  
109 might contribute to NPF events observed in the UT. Other nucleation processes combining sulfuric acid with ammonia (Kürten  
110 et al., 2016; Merikanto et al., 2007), amines (Almeida et al., 2013), di-amines (Jen et al., 2016), or organics (Kulmala et al.,  
111 2006; Metzger et al., 2010; Riccobono et al., 2014), or organics alone (Kirkby et al., 2016; Bianchi et al., 2016), have been  
112 proposed to explain some field and laboratory observations of NPF, primarily at warmer temperatures and continental  
113 locations. In a modeling study, Zhu et al. (2019) found that pure organic nucleation from biogenic volatile organic compounds  
114 could be an important source of particles, especially in the UT of modern-day pristine, continental environments and during  
115 the pre-industrial period.

116 Because there have been no in situ observations of the composition of molecular clusters and nano-particles found in  
117 convective outflow in the UT, it is difficult to ascertain which of these varied mechanisms, if any, contribute to NPF in the  
118 remote FT. In this study, we use unique observations obtained during the Atmospheric Tomography Mission (ATom), a multi-  
119 year airborne program to measure gas and aerosol properties of the remote troposphere over both the Atlantic and Pacific  
120 oceans across four seasons. Recently formed particles observed in the tropical UT were linked to recent outflow from deep  
121 convection. We use box models constrained by trajectory calculations to evaluate how well different NPF formation  
122 mechanisms can simulate the observed particle size distributions. We perform extensive model sensitivity studies to determine  
123 which nucleation mechanisms and initial precursor mixing ratios allow for the model to match observed size distributions.

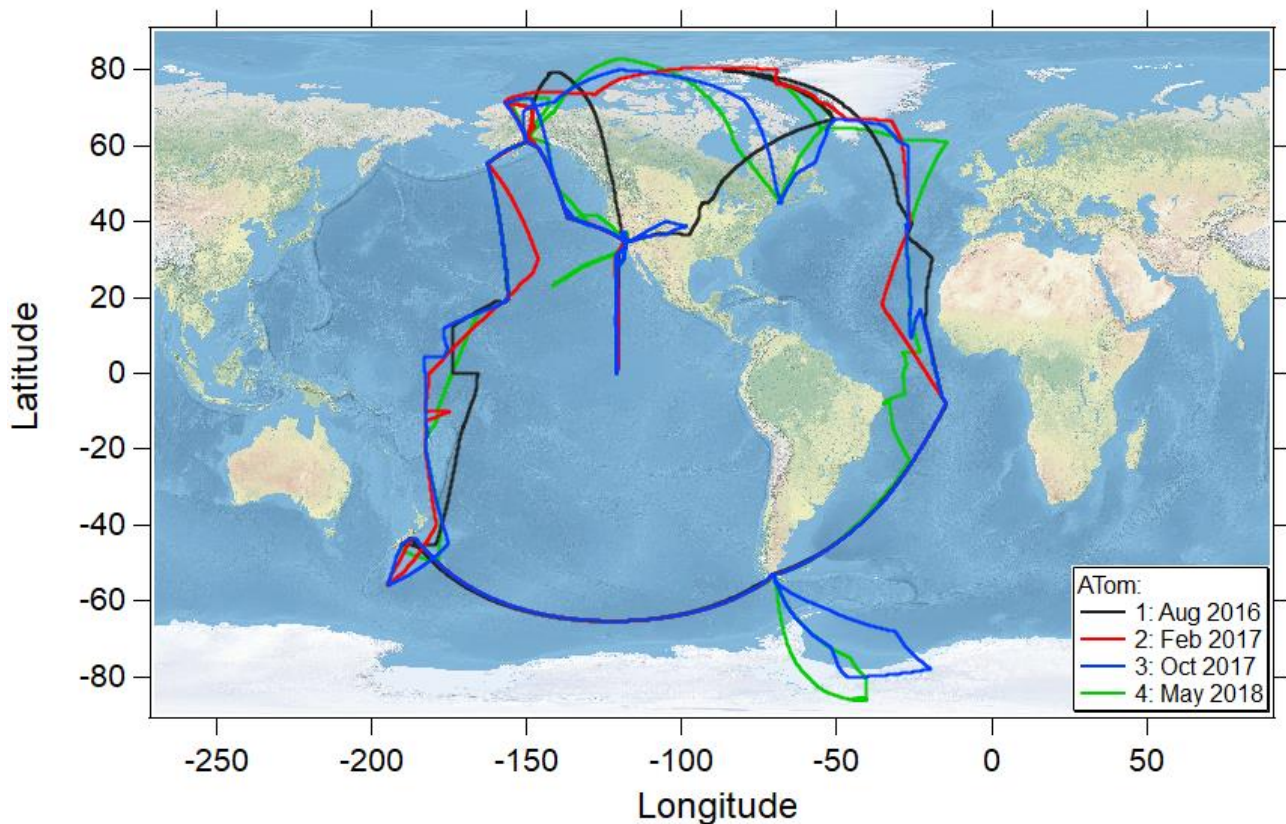
## 124 **2. Methods**

125 To establish a link between convection and NPF, and to explore the processes that govern NPF and initial growth in  
126 the tropical and subtropical free troposphere over the Pacific Ocean, we couple measured size distributions between 2.6 nm  
127 and 4.8  $\mu\text{m}$  in diameter from the four ATom missions with calculated air mass back trajectories and two box models. The back  
128 trajectories identify air masses potentially influenced by recent convection. We compare our simulations with in-situ ATom  
129 observations of aerosol size distributions. We examine which nucleation schemes best explain the observations, and evaluate  
130 whether observed sulfur precursors ( $\text{SO}_2$  and dimethyl sulfide (DMS)) can explain the NPF and the particles' initial growth.

131 In one model, we simulate particle formation by neutral and charged binary and ternary schemes, and a neutral organic scheme,  
132 and we also add organics for initial growth of the particles in all schemes. In an additional model, we form particles using both  
133 neutral and charged binary schemes.

## 134 2.1 The Atmospheric Tomography Mission

135 The NASA Atmospheric Tomography Mission (ATom) was an airborne global survey that used the NASA DC-8  
136 research aircraft to map for the first time the composition of the remote atmosphere over both the Pacific and Atlantic basins  
137 ( $\sim 82^\circ$  N to  $\sim 86^\circ$  S; Fig. 1) in nearly continuous ascents and descents between  $\sim 0.18$  and 13 km in all four seasons (July-August  
138 2016, January-February 2017, September-October 2017, and April-May 2018). The primary objectives of the mission were to  
139 examine the composition of the remote atmosphere to improve understanding of photochemical mechanisms for reactive and  
140 long-lived gas-phase species and to identify the abundance, distribution, sources of aerosol particles in the remote marine  
141 troposphere (Wofsy et al., 2018).



142  
143 **Figure 1: Flight tracks of the NASA DC-8 research aircraft during the ATom 1 (July-August 2016), ATom 2 (January-February**  
144 **2017), ATom 3 (September-October 2017) and ATom 4 (April-May 2018) missions covering the remote marine atmosphere of the**  
145 **Pacific and Atlantic Oceans between  $\sim 83^\circ$  N and  $\sim 86^\circ$  S.**

146

## 147 2.1 Measurements

148 A suite of fast time response (1 Hz) particle counters and optical particle size spectrometers were used to measure dry  
149 size distributions between 2.6 nm and 4.8  $\mu\text{m}$  in diameter (Brock et al., 2019). Two nucleation mode aerosol size spectrometers  
150 (NMASS; Williamson et al., 2018), each consisting of five continuous-flow condensation particle counters (CPCs) with  
151 different fixed cut-off diameters (i.e. diameters at which each CPC detects 50 % of the incoming particles) between 3.2 and  
152 59 nm, measured particle number concentration. Two optical aerosol counters, an ultra-high-resolution sensitivity aerosol  
153 spectrometer (UHSAS; Kupc et al., 2018) and a laser aerosol spectrometer (LAS; Froyd et al., 2019), measured particle size  
154 distributions from  $0.06 < D_p < 1 \mu\text{m}$  and  $0.12 < D_p < 4.8 \mu\text{m}$ , respectively. All concentrations reported here are corrected to standard  
155 temperature and pressure (STP), 1013 hPa and 273.15 K. The NOAA Particle Analysis by Laser Mass Spectrometry (PALMS)  
156 instrument measured the composition of individual aerosol particles (Froyd et al., 2009; 2019). For this study the PALMS size  
157 range is restricted to 0.125-1.5  $\mu\text{m}$ . Due to inlet sampling artifacts (Weber et al., 1998; Murphy et al., 2006), cloudy periods  
158 were removed from the analysis. Clouds were detected using a second-generation cloud, aerosol, and precipitation  
159 spectrometer (CAPS) mounted under the wing, which also measured coarse aerosols  $>0.5 \mu\text{m}$  (Dollner et al., in preparation)  
160 at ambient conditions.

161 Temperature, pressure, and wind speed with high time resolution (1 Hz) were measured with an accuracy of  $\pm 0.3 \text{ K}$ ,  
162  $\pm 0.3 \text{ hPa}$ , and  $\pm 1.0 \text{ m s}^{-1}$ , respectively (Scott et al., 1990). Highly sensitive sulfur dioxide ( $\text{SO}_2$ ) measurements were made  
163 during ATom 4 using laser-induced fluorescence (Rollins et al., 2016; Rollins et al., 2017) with a precision ( $1\sigma$ ) of 1-2 pptv at  
164 10 s and an overall uncertainty of  $\pm(9 \% + 2 \text{ pptv})$ . Laser-induced fluorescence was used to measure OH and  $\text{HO}_2$   
165 simultaneously (Faloona et al., 2004; Brune et al., 2020) with an accuracy of  $\pm 35 \%$ . Measurements of carbon monoxide (CO)  
166 were made using a Picarro G2401m (Chen et al., 2013) with a precision ( $1\sigma$ ) of 2-3 ppb at 10 s and an average uncertainty of  
167 4 ppb. All data used in this analysis can be found in Kupc et al. (2020).

## 168 2.2 Air mass back trajectories and convective influence

169 To identify air in the UT influenced by recent deep convection, we calculated 10-day air mass back-trajectories using  
170 the Bowman trajectory model (Bowman, 1993) driven with meteorological fields (3 hourly,  $0.25^\circ$  horizontal resolution) from  
171 the National Centers for Environmental Prediction (NCEP) Global Forecast System (GFS). Trajectories were also run with  
172 MERRA2 and ERA5 reanalysis meteorology and the results were similar. Meteorological products from NCEP interpolated  
173 to the aircraft flight track agreed best with quantities measured on the aircraft during ATom, so all analyses were done using  
174 the trajectories based on the NCEP data.

175 A cluster of 245 trajectories was initialized within a grid ( $0.3^\circ \times 0.3^\circ \times 20 \text{ hPa}$ ; Fig. S1) centered around the DC-8  
176 flight track location every minute of flight (Fig. 1). The back-trajectory time step was 3 hours, based on the reanalysis data,  
177 while a time step of 15 minutes interpolated from the 3 hours reanalysis data was used for box model simulations. Uncertainty  
178 in the back-trajectory locations is represented by the 3-D spread in the trajectory cluster. The vertical uncertainty is estimated

179 as the standard deviation in pressure (hPa) of the trajectory cluster at each time. The horizontal uncertainty is estimated using  
180 a probability grid based on the trajectory cluster in longitude and latitude at each time (Fig. S1), where probability grid refers  
181 to the number of trajectories at each time that are within each latitude-longitude grid box ( $2^\circ \times 2^\circ$ ). For instance, if 24 of the  
182 trajectories are within a certain grid box at a certain time then the probability for that grid box is  $\sim 10\%$  (24/245). The probability  
183 that air sampled by the aircraft was influenced by deep convection was calculated based on coincidences of the back-trajectory  
184 cluster with satellite derived cloud locations and characteristics such as cloud top and base pressure levels (NASA Langley).  
185 To isolate deep convection, only clouds with vertical extent  $>5$  km were considered in the convective influence (CI)  
186 calculation. The CI probability is the fraction of the trajectories in each cluster that intersected a convective system within a  
187 distance tolerance of  $0.15^\circ$  ( $\sim 10$ - $15$  km), and for which the RH with respect to liquid water ( $RH_w$ ) of the trajectory was  $>50$   
188 %. If the CI probability determined in this manner was  $>95\%$ , we assume that the aircraft was sampling air strongly influenced  
189 by deep convection.

### 190 **2.3 Description of models**

191 We use two independent aerosol nucleation and growth box models to test if different nucleation schemes are  
192 consistent with observations, following the trajectories from convective outflow to the location of the aircraft. These two  
193 models are conceptually similar, but differ in size resolution and their support for different nucleation mechanisms. Our  
194 primary model, the Two-Moment Aerosol Sectional (TOMAS; Adams and Seinfeld, 2002; Pierce and Adams, 2009; Pierce  
195 et al., 2011) includes both neutral and charged mechanisms. The neutral mechanisms include sulfuric acid and water (binary  
196 scheme; Vehkamäki et al. (2002)), sulfuric acid, water, and ammonia (ternary scheme; Napari et al. (2002)), and sulfuric acid  
197 with organics (organics scheme; Riccobono et al., 2014; Yu et al., 2017). The charged mechanism is Dunne et al. (2016),  
198 which quantifies NPF in terms of sulfuric acid, ammonia, and ion concentration (also including neutral pathways). In addition  
199 to testing the role of organics in nucleation and growth, we also test the influence of organics on aerosol initial growth when  
200 added as a condensing species following the nucleation of particles formed by each of the nucleation schemes in TOMAS, as  
201 described in Sect. 2.3.1.

202 We also use the Model of Aerosols and Ions in the Atmosphere (MAIA; Lovejoy et al., 2004; Kazil and Lovejoy,  
203 2007) to test ion-assisted nucleation of sulfuric acid and water. Since ion-assisted nucleation simulations using MAIA did not  
204 explain the observed size distributions in our work, we focus on TOMAS model description and results, and the details on the  
205 MAIA model are in the Supplemental Material (Section S1). Some features common to both models are described below.

206 The MAIA and TOMAS box models are constrained to follow the meteorological conditions along the trajectories.  
207 They are initialized at the point where the trajectories intersect deep convection, and proceed forward in time until reaching  
208 the aircraft sampling location and time. The temperature, pressure, and  $RH_w$  vary based on the trajectory. We vary the initial  
209  $SO_2$ ,  $NH_3$ , and organic aerosol precursors in TOMAS and  $SO_2$  in MAIA (Table 1 and Supplemental Material Table S1) to see  
210 which initial values of these species allow for the best matches to the observed size distribution. We note that neither model  
211 explicitly simulates DMS, which is likely to be an important aerosol precursor through its oxidation to form  $SO_2$  and

212 subsequently H<sub>2</sub>SO<sub>4</sub>, as well as through its oxidation to methanesulfonic acid (MSA; Hodshire et al., 2019), which is a  
213 condensing species that may also be able to participate in NPF (Bork et al., 2014; Chen et al., 2015; Chen and Finlayson-Pitts,  
214 2017). Previous analyses have shown that most of the observed reactive gas phase sulfur above the boundary layer is in the  
215 form of SO<sub>2</sub> (Veres et al., 2019). In this work, both models are initialized with a measurement-based, pre-existing background  
216 aerosol population that acts as a sink for condensable vapors and small particles (see Section 2.4). Nucleation-mode particles  
217 are initialized at zero concentration. We calculate the OH diurnal cycle using a prescribed peak noontime value based on  
218 observations of OH on the DC-8 aircraft (Section 2.4 and Supplemental Material Fig. S3). The OH concentration along the  
219 trajectory and the resulting production rate of H<sub>2</sub>SO<sub>4</sub> from oxidation of SO<sub>2</sub> are then calculated. We ignore possible enhanced  
220 OH due to cloud reflectivity in the vicinity of convective outflow and reduced OH from shading by higher clouds.

### 221 2.3.1 The TOMAS box model

222 The TOMAS model simulates particle nucleation, condensation, and coagulation in 43 logarithmically spaced particle  
223 size bins, which represent dry diameters from 0.7 nm-10 μm. TOMAS tracks the total aerosol number and mass of each species  
224 for each size bin. The simulated aerosol species are sulfate, ammonia, a representative oxidation product of biogenic organics,  
225 and water. In these simulations, neutral sulfuric acid-water nucleation is based on Vehkamäki et al. (2002), neutral sulfuric  
226 acid-water-ammonia nucleation is from Napari et al. (2002), ion-induced and neutral sulfuric acid-water and sulfuric acid-  
227 water-ammonia nucleation is from Dunne et al. (2016), and neutral sulfuric acid-organic nucleation is from Riccobono et al.  
228 (2014).

229 Vehkamäki et al. (2002), referred to here as VEHK, describe a parametrization for neutral sulfuric acid-water particle  
230 formation based on a classical nucleation model. They use a model for the hydrate formation relying on *ab initio* calculations  
231 of small sulfuric acid clusters and on experimental data for vapor pressures and equilibrium constants for hydrate formation.  
232 The parameterized formulas are valid at temperatures between 230.15 K and 305.15 K, RH<sub>w</sub> from 0.01%-100%, and sulfuric  
233 acid concentrations from 10<sup>4</sup>-10<sup>11</sup> cm<sup>-3</sup>. Temperatures along the trajectories ranged between 218 and 252 K and thus were  
234 below the applicable temperatures of this nucleation scheme in 18 out of 32 simulated cases. In these low-temperature cases,  
235 we assume the temperature to be 230.15 K (i.e., we do not extrapolate beyond the bounds of the parameterization). When  
236 sulfuric acid concentration was <10<sup>4</sup> molecules cm<sup>-3</sup>, the model assumes a nucleation rate of zero, and it limits the maximum  
237 concentration of gas phase sulfuric acid to 10<sup>11</sup> molecules cm<sup>-3</sup>.

238 In the Napari et al. (2002) scheme, referred to here as NAPA, the nucleation rate is parameterized using four variables:  
239 temperature, RH<sub>w</sub>, H<sub>2</sub>SO<sub>4</sub> concentration, and NH<sub>3</sub> mixing ratio. The parameterization is valid for temperatures from 240–300  
240 K, RH<sub>w</sub> from 5–95%, sulfuric acid concentrations from 10<sup>4</sup>–10<sup>9</sup> molecules cm<sup>-3</sup>, ammonia mixing ratios from 0.1–100 ppt,  
241 and nucleation rates from 10<sup>-5</sup>–10<sup>6</sup> cm<sup>-3</sup>s<sup>-1</sup>. When temperature is <240 K or >300 K (25 out of 32 simulated cases), or RH<sub>w</sub> is  
242 outside of the limits stated above, the model assumes the temperature to be 240 or 300 K, and RH<sub>w</sub> to be 5 or 95 %, respectively.  
243 When the sulfuric acid concentration is <10<sup>4</sup> molecules cm<sup>-3</sup> the model assumes a nucleation rate of zero, and it limits the  
244 maximum concentration of gas phase sulfuric acid to 10<sup>9</sup> molecules cm<sup>-3</sup>.



245 This parametrization accounts only for hydrate formation and neglects the formation of ammonium bisulfate and its  
 246 effect on nucleation rate (Zhang et al., 2010). It overpredicts the effect of ammonia on nucleation when compared with  
 247 laboratory measurements (Zhang et al., 2010). Merikanto et al. (2007) showed that nucleation rates based on the NAPA scheme  
 248 were biased high, and Lucas and Akimoto (2006) indicated that this scheme in a global model predicted unrealistically high  
 249 nucleation rates throughout the troposphere. To address these issues, Westervelt et al. (2013) and Jung et al. (2010) used a  
 250 nucleation rate tuning factor of  $1 \times 10^{-5}$  in the boundary layer and found that the model produced a reasonable agreement with  
 251 observations. In this study we performed simulations both with (NAPAt) and without (NAPA) this tuning factor.

252 In Dunne et al. (2016), referred to here as DUN, the inorganic nucleation rates determined experimentally in the  
 253 CLOUD chamber are parametrized in four dimensions: sulfuric acid, ammonia, temperature (208-292 K) and ion formation  
 254 rates ( $0-75 \text{ cm}^{-3} \text{ s}^{-1}$ ). Humidity is not included in this parametrization. The overall nucleation rate is given by the sum of the  
 255 individual processes

$$256 J_{b,n} = k_{b,n}(T)[H_2SO_4]^{p_{b,n}} \quad (1)$$

$$257 J_{t,n} = k_{t,n}(T)f_n([NH_3], [H_2SO_4]) \quad (2)$$

$$258 J_{b,i} = k_{b,i}(T)n_-[H_2SO_4]^{p_{b,i}} \quad (3)$$

$$259 J_{t,i} = k_{t,i}(T)n_-f_i([NH_3], [H_2SO_4]) , \quad (4)$$

260 where  $J_{b,n}$  is the binary neutral rate,  $J_{b,i}$  is the binary ion-induced rate,  $J_{t,n}$  is the ternary neutral rate,  $J_{t,i}$  is the ternary ion-  
 261 induced rate,  $n_-$  is the steady state concentration of small negative ions and  $[H_2SO_4]$  and  $[NH_3]$  are gas concentrations ( $\text{cm}^{-3}$ ).  
 262 In this paper, we investigated separately ion-induced binary (DUN with  $NH_3$  set to 0) scheme as well as the overall nucleation  
 263 scheme (DUN) given by the sum of the above.

264 Sulfuric acid-organic nucleation was simulated using the scheme described in Riccobono et al. (2014), referred to  
 265 here as RIC. While this scheme was developed to represent terrestrial organic species, we use it here as a surrogate for marine  
 266 organic compounds because there are no specific mechanisms that have been developed for remote marine-sourced precursors.

267 The model includes a secondary organics aerosol precursor (SOAP;  $MW=200 \text{ g mol}^{-1}$ ) variable, which can oxidize  
 268 to form a condensable aerosol species. This species can both participate in nucleation in the RIC scheme and condense onto  
 269 particles in all schemes studied here. We assume a reaction rate constant for the oxidation of biogenic organic species against  
 270 OH is  $\sim 3 \times 10^{-12} \text{ cm}^3 \text{ s}^{-1} \text{ molec}^{-1}$ , which is roughly an average reaction rate of non-methane alkanes according to Table 1 of  
 271 Atkinson and Arey (2003). This rate constant gives a SOAP lifetime of  $\sim 2$  days for a typical diurnally averaged UT OH  
 272 concentration of  $2 \times 10^6 \text{ cm}^{-3}$ . The yield of SOAP to secondary organic aerosol (SOA) is set to 1, which allows us to use SOAP  
 273 as a simple, tunable variable to determine how much SOA may be necessary to match observed aerosol formation and growth.  
 274 We use the SOAP oxidation product (i.e. condensable organic) in the RIC scheme, but also use it to explore the effects of  
 275 organics on new particle growth for each of the nucleation schemes (Riipinen et al., 2011).

276 In the RIC mechanism, nucleation occurs when only a fraction of the oxidation products of biogenic organic  
 277 compounds (*BioOxOrg* in the terminology of the RIC mechanism), formed from SOAP oxidation, are able to form stabilized

278 clusters. The formation rate dependence on sulfuric acid and *BioOxOrg* concentration is given by a fit to experimental data in  
279 the form

$$280 \quad J_{ORG} = k_{NUC}[H_2SO_4]^p[BioOxOrg]^q, \quad (5)$$

281 where  $J_{ORG}$  is the formation rate ( $\text{cm}^{-3}\text{s}^{-1}$ ) of stable particles with diameters  $\sim 1.7\text{nm}$ ,  $k_{NUC}$  is the nucleation rate constant with  
282 a value of  $3.27 \times 10^{-21} \text{ cm}^6 \text{ s}^{-1}$  at 278 K and  $\text{RH}_w$  at 39 %, *BioOxOrg* represents concentration of later generation oxidation  
283 products of biogenic monoterpenes ( $\text{cm}^{-3}$ ), and the exponents  $p=2$  and  $q=1$  represent the power law dependence of  $J_{ORG}$  upon  
284 the concentrations of sulfuric acid and *BioOxOrg*.

285 Using the RIC scheme, we test the effect of different fractions of condensable organic formed from SOAP oxidation.  
286 This fraction,  $F_{orgnuc}$  represents the fraction of the condensable *BioOxOrg* that may participate in nucleation by stabilizing the  
287 cluster. The value of  $F_{orgnuc}$  does not affect the condensation of organics onto already-nucleated or pre-existing particles. Using  
288  $F_{orgnuc}$  allows us to decouple the possible role of organics in nucleation vs. their role in subsequent condensational growth.

289 Since RIC scheme does not consider the possible effect of temperature on the nucleation rate, we modify the  
290 nucleation rates predicted in equation (5) using the temperature dependence (270-310 K) for this nucleation rate from Yu et  
291 al. (2017)

$$292 \quad J_{ORG-T} = J_{ORG} f_T \quad (6)$$

$$293 \quad f_T = \exp \left[ \frac{\Delta H}{k} \left( \frac{1}{T} - \frac{1}{T_0} \right) \right], \quad (7)$$

294 where  $f_T$  is the nucleation rate scale factor accounting for the temperature dependence, and  $\Delta H$  is the change in enthalpy of -  
295  $38.3 \text{ kcal mol}^{-1}$  associated with the critical cluster formation. We assume that  $\Delta H$  is constant throughout our full temperature  
296 range.

297 One of the limitations of our box modeling effort is that the temperatures along the trajectories ranged between 218  
298 and 252 K, often below the applicable temperatures of the three nucleation schemes: VEHK, NAPA and RIC (Supplemental  
299 material Table S2). We would expect faster nucleation rates at the lower trajectory temperatures than are simulated by these  
300 schemes (e.g. Yue and Hamill, 1979). Using VEHK and NAPA schemes below their lower temperature limit means forcing  
301 them to their lowest rated temperature 230.15 K and 240 K respectively. This in turn may result in underestimating particle  
302 concentration and size. This bias for cold cases means that VEHK and NAPA schemes may predict  $\text{SO}_2$  and organic precursors  
303 that would be anomalously high. In the RIC scheme the temperature dependence of Yu et al. (2017) is not experimentally  
304 verified down to the tropical UT temperatures. Thus, we tested the impact of changing the  $\Delta H$  by  $\pm 3 \text{ kcal mol}^{-1}$  (Supplemental  
305 material Fig. S2). We also have not explored the organic-only nucleation scheme by Kirkby et al. (2016).

## 306 2.4 TOMAS input data

307 Measured and estimated inputs needed to initialize the TOMAS box model (Adams and Seinfeld, 2002; Pierce and  
308 Adams, 2009; Pierce et al., 2011) are given in Table 1. TOMAS was configured to use measured size distributions ( $>12 \text{ nm}$ )  
309 in discrete bins. Each input in Table 1 represents the initial conditions present at the start of the simulation ( $t_0$ ). Hence,

310 condensing vapor in the gas phase can contribute both to the formation and growth of new particles and growth of the pre-  
311 existing background aerosol.

312 We expect the output of the TOMAS model to be sensitive to the temperature dependence of nucleation rates, the  
313 type and number of organic compounds, SO<sub>2</sub>, OH, NH<sub>3</sub> mixing ratios, and the pre-existing background aerosol into which the  
314 convective outflow is mixed. The variability of the simulated aerosol size distribution to various initial conditions was  
315 examined by conducting sensitivity simulations (Table 1) on SO<sub>2</sub>, NH<sub>3</sub>, OH, background aerosol size distribution, organics  
316 added for initial growth (e.g., SOAP), and on the RIC scheme scale factor  $F_{orgnuc}$  for organics involved in cluster formation.

317 The pre-existing aerosol is estimated based on the 1-minute averaged size distributions for  $D_p > 12$  nm as observed at  
318 the aircraft location. The concentration of particles with  $D_p < 12$  nm is set to zero under the assumption that these particles were  
319 produced by the new particle formation being modeled and were not present in the background air at the point of mixing with  
320 the air detrained from convection. The box model simulations do not explicitly account for the mixing of highly scavenged air  
321 detraining from convective outflow with surrounding UT air containing more aged aerosol (e.g., Weigel et al. 2011). We have  
322 undertaken sensitivity studies that vary the pre-existing background aerosol used as initial input parameter (Table 1).

323 The box model simulations were run forward in time from the moment the parcel exited the convection ( $t_0$ ) to the  
324 point of measurement by the aircraft ( $t_{fin}$ ), with temperature, pressure, and RH<sub>w</sub> varying as a function of time as determined  
325 from the back trajectory. The change in RH<sub>w</sub> along the trajectory between the trajectory location at the cloud edge ( $t_0$ ) and the  
326 point of the aircraft location ( $t_{fin}$ ) for 32 simulated cases is presented in Fig. S67. The concentration of OH at solar zenith angle  
327 of 0° in the simulations was set to  $3 \times 10^6$  molecules cm<sup>-3</sup>; however, we also tested OH concentrations of  $1 \times 10^6$  and  $4.3 \times 10^6$   
328 molecules cm<sup>-3</sup>. These estimates agree well with aircraft-measured concentrations (Supplemental Material Fig. S3) and with  
329 values given in Seinfeld and Pandis (2006). In TOMAS, OH is parameterized as a function of the cosine of the solar zenith  
330 angle, where the night-time OH is  $1 \times 10^5$  molecules cm<sup>-3</sup>. The solar zenith angle is calculated for the time, altitude, latitude,  
331 and longitude of the back trajectories.

332 The SO<sub>2</sub> and NH<sub>3</sub> mixing ratios were varied between 1 and 100 pptv to explore a large range of plausible conditions.  
333 The evaluated SO<sub>2</sub> range exceeds that measured on ATom 4 (Supplemental Material Figs. S4 and S5) and covers the <30 pptv  
334 mixing ratios previously reported in the UT over the central and western tropical Pacific (Thornton et al., 1997; Rollins et al.,  
335 2017; Rollins et al., 2018). Organic aerosol precursors are unknown in the UT and were not directly measured; thus we explored  
336 a range of probable mixing ratios between 1 and 100 pptv.

337  
338  
339  
340  
341  
342

343 Table 1. Ranges of parameters used for sensitivity studies in the TOMAS box model. Values varied to match the observed size  
 344 distribution in *italic*).

Parameter		Initial value used
Abbreviation	Unit	TOMAS
SO <sub>2</sub> *	pptv	<i>1-100</i>
NH <sub>3</sub>		<i>1-100</i>
Secondary organic aerosol precursors (SOAP)		<i>1-100</i>
<i>F<sub>organic</sub>**</i>	%	<i>10, 50, 100</i>
OH at solar zenith angle of 0°	molecule cm <sup>-3</sup>	<i>1x10<sup>6</sup>, 3x10<sup>6</sup>, 4.3x10<sup>6</sup></i>
OH at night		<i>1x10<sup>5</sup></i>
Napari et al. (2002) scheme; nucleation rate tuning factor 1x10 <sup>-5</sup>		tuning factor on/off
Time since CI	hours	0.4-23.3
Ion pair production rate	cm <sup>-3</sup> s <sup>-1</sup>	15***
Background pre-existing aerosol: initial input size distribution (SD)		Varied measured initial input size distribution: ****SD>12nm, SD>12nm x2, SD>12nm /2, SD=0, SD>12nm-5nm, SD>8nm, SD as logarithmic fit

345 \* SO<sub>2</sub> measured on ATom 4 only

346 \*\* fraction of SOAP participating in nucleation when using Riccobono et al. (2014) in TOMAS.

347 \*\*\* value typical for the tropical upper troposphere (Dunne et al., 2016)

348 \*\*\*\* initial background aerosol size distribution was varied: SD>12nm means background SD as described in the text was used to initiate the  
 349 model; SD>12nm x2 means background SD multiplied by 2; SD>12nm /2 means SD divided by 2; SD=0 means no background aerosol;  
 350 SD>12nm-5nm means SD was shifted by 5 nm to smaller diameters; SD>8nm means measured background SD >8nm was used as initial  
 351 SD. Where SD refers to the number size distribution dN/dlog<sub>10</sub>D<sub>p</sub>.

352

## 353 2.5 Evaluating simulated size distributions

354 To determine which sets of parameters allow the models to reproduce the observed size distributions best, we evaluate  
 355 every simulation against observations using the normalized mean error (*NME*) statistic of the first four moments (0<sup>th</sup> through  
 356 3<sup>rd</sup>) of the size distribution for each model simulation as

$$357 \quad NME = \frac{\sum_{i=0}^3 \frac{|S_i - O_i|}{O_i}}{4}, \quad (8)$$

358 where  $S_i$  and  $O_i$  are  $i^{\text{th}}$  moments of the simulated and observed size distributions, respectively (Hodshire et al., 2018).

359 The  $i^{\text{th}}$  moment is defined as

$$360 \quad M_i = \int_{2.6}^{20} n_N D_p^i dD_p, \quad (9)$$

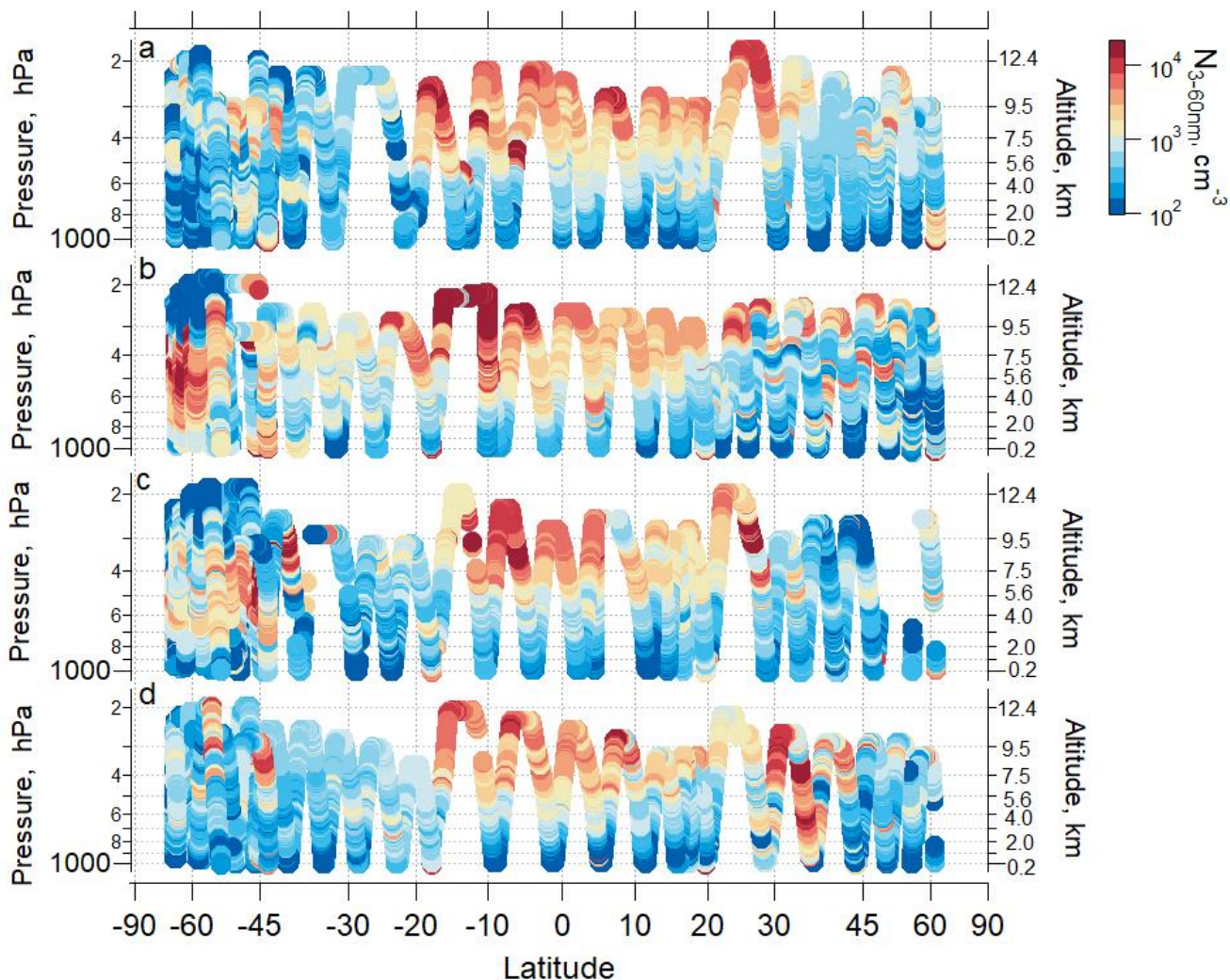
361 where  $n_N$  is the number of particles in size interval  $dD_p$  and  $D_p$  is the diameter. Equation (9) is integrated over the diameter  
 362 range from 2.6-20 nm, and  $M_i$  represents either  $S_i$  or  $O_i$ . The zeroth moment ( $i=0$ ) corresponds to the number of particles, the  
 363 first moment ( $i=1$ ) to the total diameter of particles (i.e. total aerosol length), the second moment ( $i=2$ ) is proportional to the  
 364 total surface area of particles, and the third moment ( $i=3$ ) is proportional to the total volume of particles. A *NME* of 0 is a  
 365 perfect fit between the simulation and observations; a *NME* of 1.0 indicates that the average bias of the 0<sup>th</sup> through 3<sup>rd</sup> moments

366 between the simulation and observations is 100%. As the *NME* is given as an absolute value, we do not discriminate between  
367 cases in which the model is underpredicting or overpredicting the moments on average. Since these moments are equally  
368 weighted, a low value of *NME* can be achieved only if the modeled size distribution accurately simulates both the shape and  
369 magnitude of the observed size distribution over the full range of sizes evaluated.

### 370 **3. Results**

#### 371 **3.1 Observations**

372 Our data show seasonally persistent high nanoparticle concentrations over the remote tropical UT (Fig. 2; Williamson  
373 et al., 2019). In this region, the highest concentrations of particles were in the nucleation mode (3-12 nm), which have a short  
374 lifetime and are the products of recent NPF. This tropical UT feature was observed in all ATom deployments over all four  
375 seasons, over both the Pacific and Atlantic basins. The concentrations of particles observed in the UT over the tropical Atlantic  
376 were lower in concentration than observed over the Pacific (Supplemental Material Fig. S6). In this study, we focus on  
377 observations over the remote Pacific, which is a region less perturbed by continental emissions than the Atlantic (Fig. 3 and  
378 Supplemental Material Fig. S7 and S8).



379

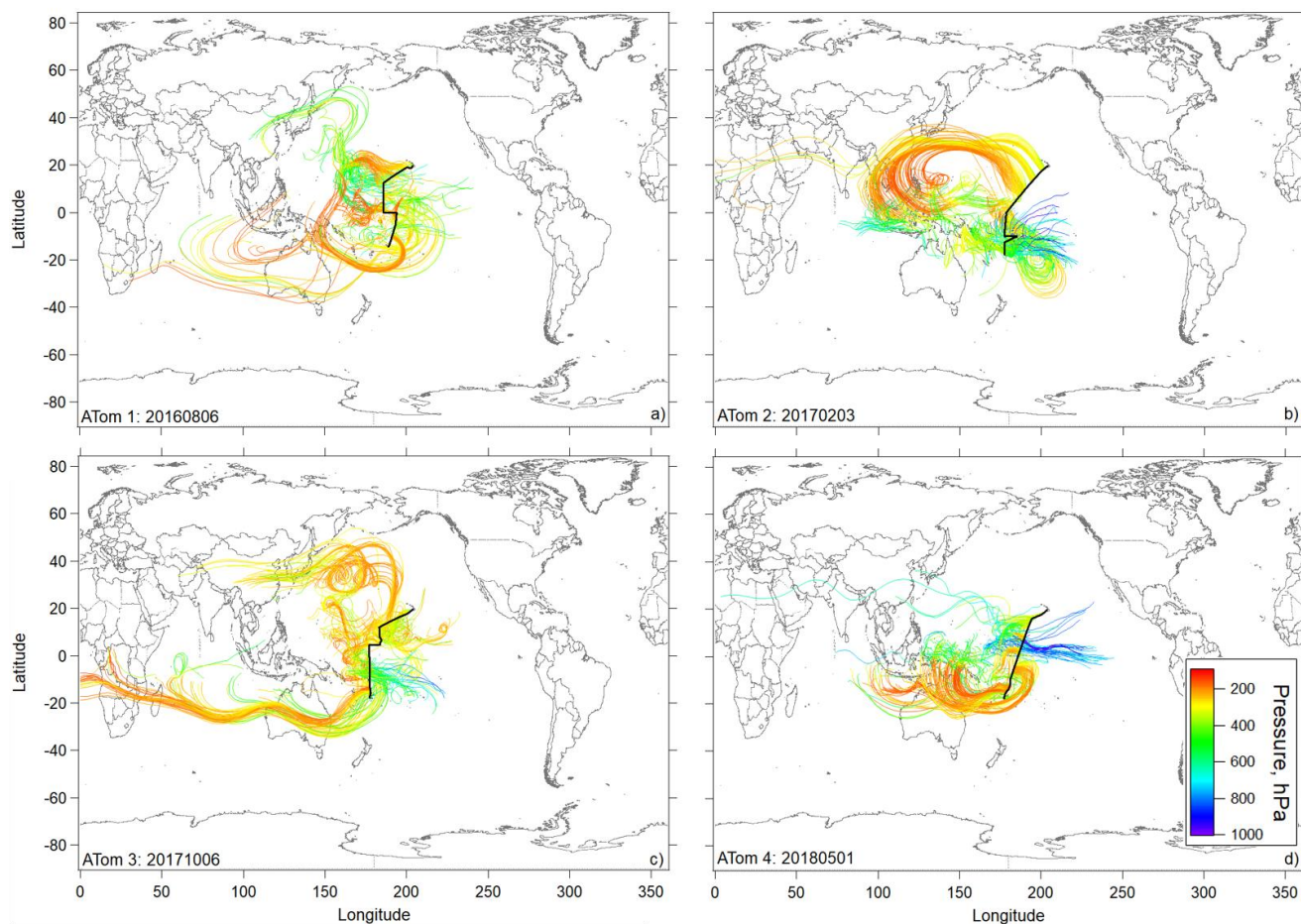
380 **Figure 2: Ambient pressure as a function of latitude colored by the measured number concentration of particles with  $D_p$  from 3 - 60**  
 381 **nm over the Pacific Ocean for a) ATom 1, July-August 2016; b) ATom 2, January-February 2017; c) ATom 3, September-October**  
 382 **2017; and d) ATom 4, April-May 2018). Periods of flight in clouds, over continents and near airports have been removed.**

383

384 Previous studies (e.g. Clarke, 1992, 1993; Clarke et al., 1998, 2006; Brock et al., 1995; Weber et al., 1995; Raes et  
 385 al., 1997; Thornton et al., 1997; Weber et al., 1998; Clarke and Kapustin, 2002; Twohy et al., 2002; Froyd et al., 2009;  
 386 Borrmann et al., 2010; Weigel et al., 2011) have provided strong evidence of NPF in the tropical UT and its link to convective  
 387 activity. However, these earlier studies did not provide such extensive, representative, and global-scale coverage of the remote  
 388 marine troposphere over a wide range of altitudes and latitudes (Williamson et al., 2019). The ATom observations also provide  
 389 accurate and sensitive, state-of-the-science measurements of the chemical composition of the bulk aerosol and the abundance  
 390 of hundreds of gas-phase species in all four seasons, making these observations the most comprehensive to date. However, no

391 measurements were made during ATom of  $\text{NH}_3$ , the highly oxygenated organic molecules that are likely aerosol precursors,  
392 or molecular cluster composition, and measurements of  $\text{SO}_2$  took place only during the fourth ATom deployment.

393 Ten-day back trajectories in the region of NPF in the central Pacific showed transport primarily over the Pacific, with  
394 some possible terrestrial influence from the western Pacific region (Fig. 3). However, trajectories coming from the western  
395 Pacific generally stayed at high altitudes and did not show recent convective uplift from regions influenced by terrestrial  
396 sources. Further, CO and other continental tracers were at background levels over the Pacific, confirming little continental  
397 influence in the sampled air masses (Supplemental Material Fig. S7), as opposed to the Atlantic (Supplemental Material Fig.  
398 S6 and S7). Thus, the precursors of the recently formed particles are likely mostly marine in origin. The latter is also supported  
399 by the measurement of particle phase methanesulfonic acid (MSA) that can be considered as a tracer for maritime influence  
400 on the tropical UT (Fig. S9).

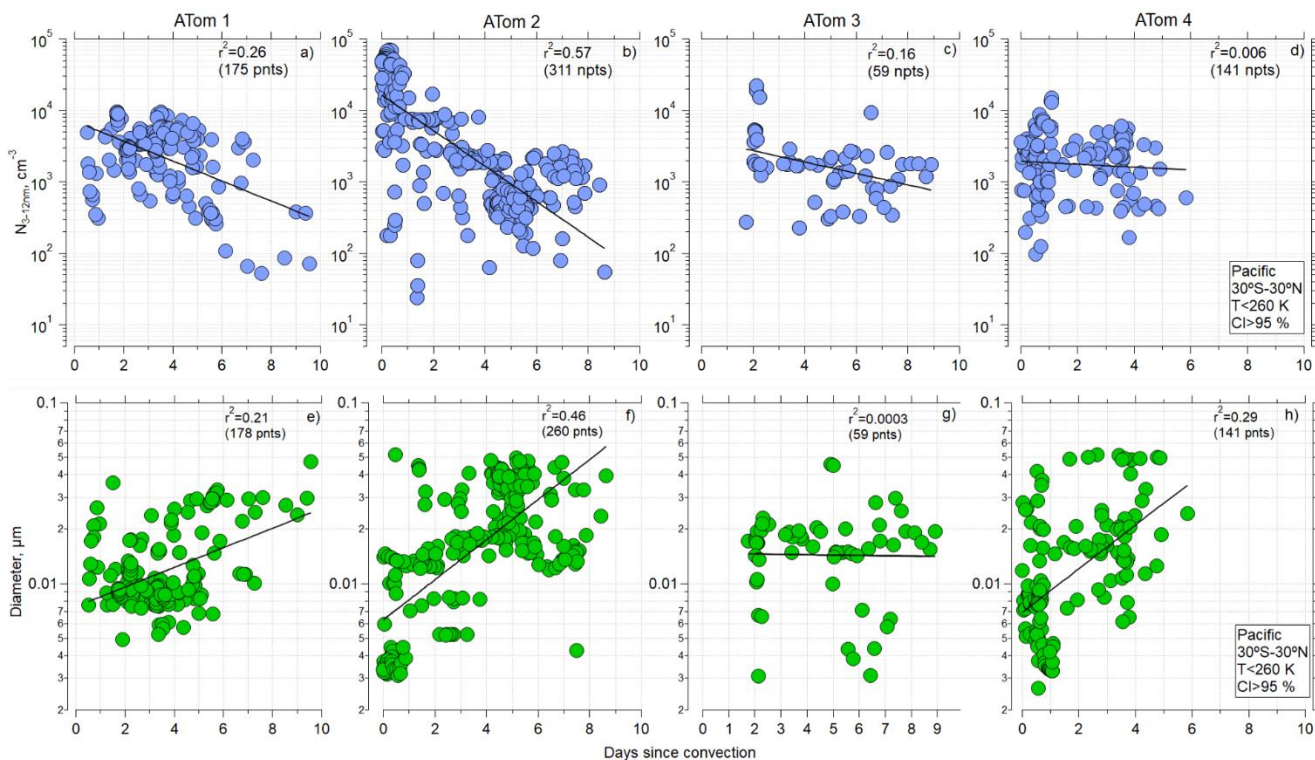


401  
402 **Figure 3: Flight track and selected 10-day back trajectories initiated for times in flight at pressures <400 hPa (<~260 K) sampled**  
403 **along the DC-8 flight track during ATom 1, 2 (a, b), 3 and 4 (c, d) during the most tropical flight in each deployment (Hawaii-Samoa**  
404 **on ATom 1 and Hawaii-Fiji on ATom 2-4). Trajectories are colored according to the pressure along their pathway.**

405



406 The observations and trajectory modeling show that newly formed particles were often associated with deep  
 407 convection. Similar trajectory analyses, in terms of examining the history of the sampled air masses for interactions with deep  
 408 convection, have been undertaken by Froyd et al. (2009) and Andreae et al. (2018). Here, using the CI probability criterion of  
 409 95% to identify when the aircraft was sampling air recently influenced by convection (Sect. 2.2), and considering the latitude  
 410 range 30° S - 30° N and ambient temperatures <260 K, for ATom 1 and 2, the shorter the time since convection, the higher the  
 411 number of small particles (Fig. 4a-d). Such strong trends were not evident for ATom 3 and 4 indicating that factors other than  
 412 time since CI affect nucleation-mode concentrations. The more recent the convection, the smaller the diameter of the nucleation  
 413 mode (Fig. 4e-h). These relationships are again strongest for ATom 1 and 2 and also 4. Our hypothesis for these relationships  
 414 is that with increasing time since CI, particles with diameters <12 nm grew by condensation and coagulation and decreased in  
 415 concentration by coagulation, leading to the decrease in nucleation-mode concentration and increase in diameter. A similar  
 416 trend was observed over the Atlantic (Supplemental Material Fig. S10). The highest concentrations of nucleation-mode  
 417 particles occurred during ATom 2 and were associated with the shortest times since CI.  
 418

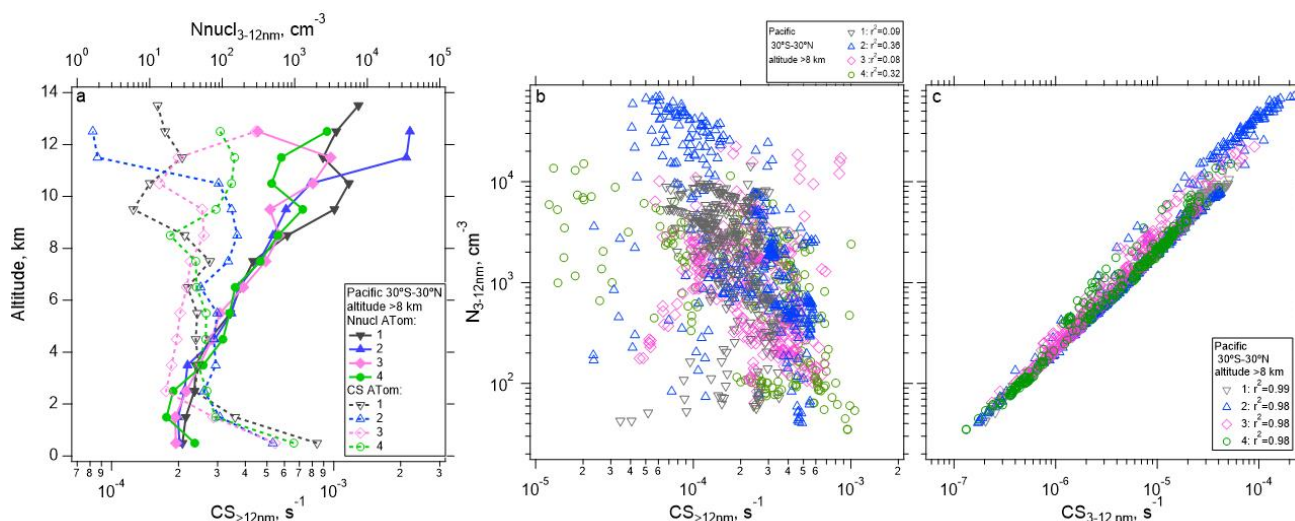


419  
 420 **Figure 4: (a-d) Concentration of nucleation mode particles as a function of time since convective influence for ATom 1-4, over Pacific**  
 421 **(30° S - 30° N), T<260 K and probability of convective influence >95 %, respectively. (e-h) Modal diameter of particles with  $D_p < 0.06$**   
 422  **$\mu\text{m}$  as a function of time since convective influence (30° S - 30° N) for ATom 1-4, respectively. Black line, used to guide the eye,**  
 423 **represents the linear regression fitted to log-y values. A corresponding Pearson correlation coefficient  $r^2$  is indicated.**

424



425 Air detraining from deep convection is likely depleted in pre-existing particles due to in-cloud removal, leading to a  
 426 reduced condensation sink (CS) that enhances the likelihood of NPF (e.g., Clarke, 1992; Williamson et al., 2019). Figure 5  
 427 shows the concentration of measured nucleation-mode particles as a function of altitude for the Pacific basin over four ATom  
 428 missions. The median concentration of nucleation mode particles averaged from 30° S to 30° N is highest at altitudes >10 km,  
 429 reaching  $\sim 40,000 \text{ cm}^{-3}$  (Fig. 5a), coinciding with the lowest values of  $\text{CS}_{>12\text{nm}}$ , which competes with NPF for condensing  
 430 vapors. The CS term is calculated for particle diameters >12 nm, and for the diameter range between 3 and 12 nm following  
 431 Williamson et al. (2019).  $\text{CS}_{>12\text{nm}}$  serves as an estimate of the condensation sink prior nucleation starting, and it is negatively  
 432 correlated with the number of nucleation mode particles (Fig. 5b), while the nucleation mode is positively correlated with  $\text{CS}_{3-12\text{nm}}$   
 433 (Fig. 5c). Over the Atlantic, the maximum concentration of nucleation-mode particles >8 km in altitude averaged from  
 434 30° S to 30° N,  $\sim 3,000 \text{ cm}^{-3}$ , is considerably smaller than over the Pacific, but the shape of the profile is similar (Fig. S11).



435 **Figure 5. a) Vertical profile of the median number concentration of nucleation mode particles (3-12 nm) and condensation sink (CS)**  
 436 **averaged between 30° S - 30° N as a function of altitude for the four ATom deployments. (b-c) One minute average nucleation mode**  
 437 **particle concentrations at >8 km in altitude as a function of  $\text{CS}_{>12\text{nm}}$  (b) and  $\text{CS}_{3-12\text{nm}}$  (c), between 30° S - 30° N over the Pacific Ocean.**  
 438 **Pearson correlation coefficient values ( $r^2$ ) are indicated in the legend.**

439 Some variability in the strength of NPF and its dependence on  $\text{CS}_{>12\text{nm}}$  can be observed. In general,  $\text{CS}_{>12\text{nm}}$  is weakly  
 440 negatively correlated ( $r^2$  between 0.08 and 0.36 depending on the ATom mission) with the concentration of nucleation mode  
 441 particles (Fig. 5b), as would be expected if NPF were competing with  $\text{CS}_{>12\text{nm}}$  for condensing vapors. When CS is dominated  
 442 by small particles ( $\text{CS}_{3-12\text{nm}}$ ) the correlation is strongly positive ( $r^2$  between 0.97-1, Fig. 5c). Factors other than CS are also  
 443 important in controlling the concentrations of newly formed particles. These factors may include temperature and  $\text{RH}_w$ , actinic  
 444 flux, and OH that drive photochemical reactions that oxidize precursor species, the abundance of those precursor species in

445 the air lifted by convection and in the background air, and the time since the air parcel exited a convective cloud (Figs. S12-  
446 S13).

### 447 3.2 Box model simulations

448 Case studies were selected for box model simulations based on specific criteria such as temperature and CI  
449 probability. We restrict the analysis to data taken nominally in the tropics and subtropics, between 30° S - 30° N latitude. We  
450 consider the case for analysis by box modeling if the CI probability is >95%, temperature at the point of measurement is <260  
451 K, and an aerosol number mode with a modal peak diameter <12 nm is present (Table 2). We performed simulations for 32  
452 cases randomly selected from the ATom 2 (20 out of 47 identified cases) and ATom 4 (12 out of 60 identified cases) datasets  
453 over the remote tropical Pacific from the total number of 109 cases with time since convection <1 day (Table 2). Data from  
454 ATom 2 and ATom 4 were selected for simulations because these deployments had the most identified cases with time since  
455 CI <1 day. During ATom 2, we observed the highest numbers of nucleation mode particles, lowest condensation sink, and  
456 shortest time since convection (Fig. 5) among all missions. Measurements of SO<sub>2</sub> mixing ratio were made only during the  
457 ATom 4 deployment, providing an important constraint for the box model simulations. We did not perform simulations on  
458 ATom 1 and ATom 3 data as there were only 2 and 0 identified cases with time since CI <1 day, respectively (Table 2).

459 The correlation between nucleation-mode particles and time since CI was strongest in ATom 2 (Fig. 4), while CO  
460 levels, a proxy for continental influence, were the lowest for trajectory times <1 day (Supplemental Material Fig. S7). Although  
461 SO<sub>2</sub> was not measured during ATom 2, we expect SO<sub>2</sub> in this region in the UT to be <30 pptv based on SO<sub>2</sub> levels measured  
462 during ATom 4 and other missions in the Pacific (Supplemental Material Figs. S4, S5).

463

464 Table 2. Number of identified cases of recent NPF associated with CI for the Pacific (Atlantic in Table S4) between 30° N and  
465 30° S latitude that meet the following criteria: T<260 K, CI > 95%, and modal peak diameter < 12 nm.

ATom mission	Number of cases meeting selection criteria		
	Trajectory age <1 day	Trajectory age 1-2 days	Trajectory age 2-3 days
1	2	20	49
2	47	3	4
3	0	0	5
4	60	9	2
Total	109	32	60

466

467 The size distributions simulated by TOMAS were smoothed to avoid the artificial distortion of the distribution caused  
468 through size-bin emptying (Hodshire et al., 2019; Stevens et al., 1996). The latter and the smoothing technique are described  
469 in Supplemental Material Section S2.

470 We performed box model simulations on the 32 selected cases using the range of values listed in Table 1. The success  
471 of each model simulation was evaluated using the *NME* described by Eq. 8. As an example using a single case, Fig. 6a shows  
472 the observed and simulated aerosol size distribution with the best *NME* obtained for each of the various nucleation schemes  
473 tested, along with the corresponding mixing ratios of SO<sub>2</sub>, NH<sub>3</sub>, or organics. Organics here refer to the SOAP oxidation product  
474 (i.e. condensable organic) that participates in nucleation in the RIC scheme (as *BioOxOrg*), and in the particle condensational  
475 growth in all schemes. The value of *NME* as a function of the mixing ratios of SO<sub>2</sub>, NH<sub>3</sub>, and organics for each nucleation  
476 scheme is also shown (Fig. 6b-j). The summary of each of the 32 simulated cases is presented in Supplemental Material Table  
477 S4 and Figs. S15-S45. The simulations in Fig. 6 used the default OH scheme with a maximum concentration of 3x10<sup>6</sup> cm<sup>-3</sup> at  
478 a solar zenith angle of 0° (Supplemental Material Fig. S3). Sensitivity studies for maximum OH values of 1x10<sup>6</sup>, 3x10<sup>6</sup> and  
479 4.3x10<sup>6</sup> cm<sup>-3</sup> are presented in Supplemental Material Fig. S46-S50.

480 TOMAS simulations using VEHK scheme substantially underpredict the observed tropical nucleation-mode number  
481 concentration, with resulting poor values of *NME* (Fig. 6). Sensitivity tests that vary the pre-existing initial (background)  
482 aerosol or completely remove background particles do not change the results significantly (Supplemental Material Fig. S51-  
483 S53). Further, we find that changing initial input parameters such as SO<sub>2</sub> and OH as indicated in Table 1 do not improve the  
484 *NME* for VEHK scheme (Fig. 6b; Supplemental Material Fig. S46). Adding organics to grow particles nucleated by the VEHK  
485 scheme, while reducing *NME* slightly, does not provide adequate agreement with the observations. Varying the pre-existing  
486 initial aerosol or completely removing background particles in VEHK scheme with added organics may improve the fits for  
487 certain initial conditions (Fig. S52), making it plausible for better *NME* values if CS<sub>>12nm</sub> was 4.12x10<sup>-5</sup> s<sup>-1</sup>, SO<sub>2</sub> and organics  
488 were 13.9 pptv and 7.2 pptv, respectively, for this particular case. Out of 32 cases studied here, there is no case with *NME*  
489 <0.2 for VEHK scheme. Similarly, the ion-assisted binary nucleation scheme of the MAIA box model does not provide good  
490 matches with observations (Supplemental Material Table S4).

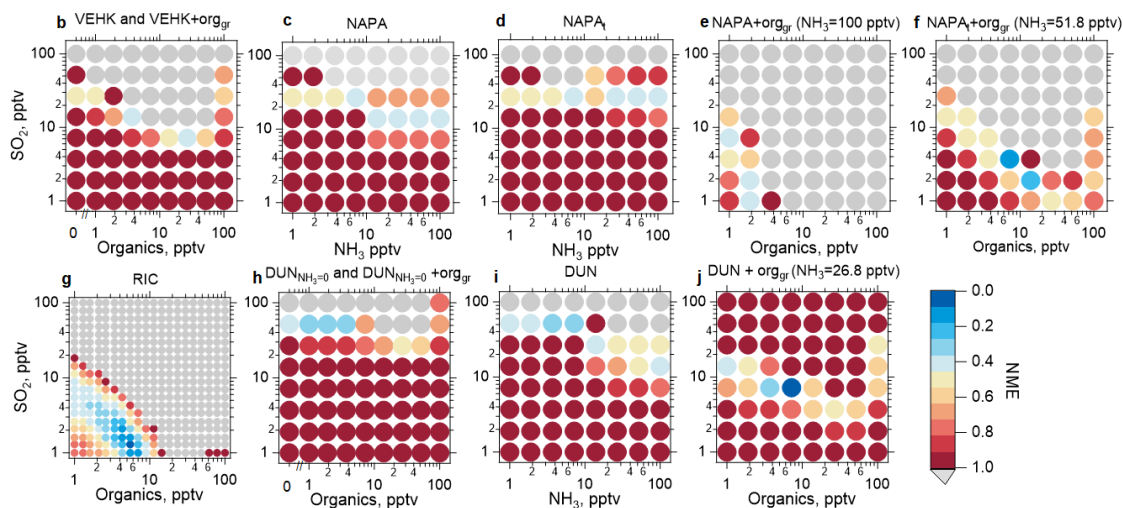
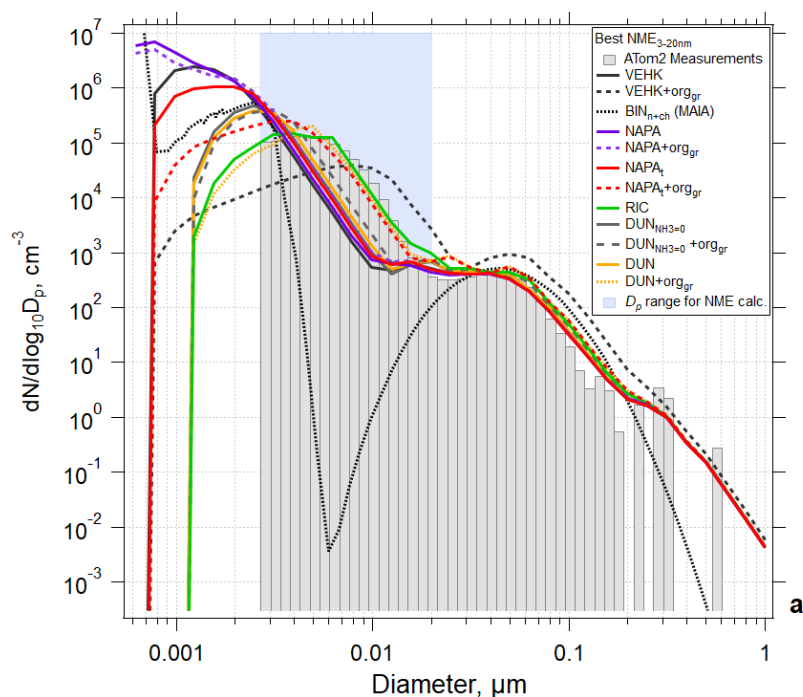
491 The NAPA scheme, both with (NAPAt) and without (NAPA) the tuning factor, did not significantly reduce the *NME*  
492 values from the VEHK results for this case (Fig. 6c). However, when organics were added to condense on the particles  
493 nucleated by this mechanism, the *NME* improves, resulting in 6 cases with *NME* <0.2 (Table S4). The RIC nucleation scheme,  
494 updated by the temperature dependence of Yu et al. (2017), provides the best *NME* (*NME*=0.02) for all the schemes  
495 investigated (Fig. 6f) for the case shown in Fig. 6. We explored this mechanism with 6 more sensitivity simulations, including  
496 various combinations of initial SO<sub>2</sub> and organic mixing ratios, to see how sensitive *NME* is to small changes of initial precursor  
497 vapor mixing ratios. For the example case presented in Fig. 6a, organic mixing ratios <10 pptv and SO<sub>2</sub> mixing ratios <5 pptv  
498 were sufficient to produce size distributions that matched the observations with good fidelity (*NME* =0.02). Varying the scale  
499 factor of organics taking part in nucleation (*F<sub>orgnuc</sub>*) did not change the results significantly (Supplemental Material Fig. S48).  
500 Nucleation can have strong self-regulating mechanisms, and these are likely contributing here. Increasing *F<sub>orgnuc</sub>* increases the  
501 nucleation rate initially in the high- *F<sub>orgnuc</sub>* simulations, which increases the condensation and coagulation sinks, which  
502 decreases the vapor concentrations (and hence nucleation and growth rates), and increases the coagulation loss rates. Each  
503 of these feedbacks lead to a buffering of changes to the nucleation mode. Westervelt et al., (2014) describes these buffering

504 mechanisms in detail. Changing  $F_{organic}$  does not change the amount of organic material and sulfuric acid that condenses though,  
505 so ultimately the size distributions are relatively insensitive to changing  $F_{organic}$  because the buffering mechanism and total  
506 condensation remain approximately constant. The most recently developed NPF mechanism, the ion-induced sulfuric acid-  
507 water, referred here as DUN with  $NH_3$  set to 0, and the sulfuric acid-water-ammonia (DUN) nucleation scheme from Dunne  
508 et al. (2016), did not provide the lowest *NME* values among the schemes tested, although adding organics for initial growth of  
509 the nucleated particles improved the fits ( $NME=0.04$ ) (Fig. 6i, Supplemental Material Table S4). The addition of organics  
510 resulted in best *NME* values for DUN in 5 out of the 32 cases simulated.

511 Overall, a reduction in *NME* when organics are added for initial particle growth was also observed for other schemes  
512 (Supplemental Material Table S4). Out of 32 case studies, we found 6 cases when the NAPAt with organics for growth and  
513 the tuning factor applied gave lower *NME* values than all other schemes. However, 4 out of these 6 cases require  $SO_2$  or  $NH_3$   
514 mixing ratios  $>50$  pptv that exceed ATom 4  $SO_2$  observations and literature values in the tropical UT for  $SO_2$  of  $<30$  pptv (Fig.  
515 S4; (Rollins et al., 2017, 2018; Thornton et al., 1997) and for  $NH_3$  of  $<10$  pptv (Höpfner et al., 2016; Feng and Penner, 2007;  
516 Adams et al., 1999).

517 Growth rates calculated basing on the diameter of the leading edge and threshold value of  $dN/d\log_{10}D_p > 10 \text{ cm}^{-3}$  in  
518 any of the size bins below 12 nm were mostly between 0.1 and 3  $\text{nm hr}^{-1}$  for the RIC scheme (Figure S71). The growth rates  
519 for all cases investigated here using RIC and other schemes are presented in Figure S72.

520  
521  
522  
523



	VEHK*	VEHK*+org <sub>gr</sub>	BIN <sub>ch</sub> (MAIA)	RIC*	NAPA*	NAPA*+org <sub>gr</sub>	NAPA*+org <sub>gr</sub>	NAPA*+org <sub>gr</sub>	DUN <sub>NH3=0</sub>	DUN <sub>NH3=0</sub> +org <sub>gr</sub>	DUN	DUN+org <sub>gr</sub>
NME <sub>3-20nm</sub>	0.48	0.41	0.73	0.02	0.42	0.38	0.39	0.17	0.37	0.30	0.34	0.04
SO <sub>2</sub> , pptv	26.8	7	26.8	1.3	13.9	7.2	26.8	3.7	51.8	51.8	51.8	7.2
Organics, pptv		26.8		5.5		1		7.2		1		7.2
NH <sub>3</sub> , pptv					13.9	100	100	51.8			7.2	26.8

\*Temperature along the trajectory does not lie within the temperature range of the scheme

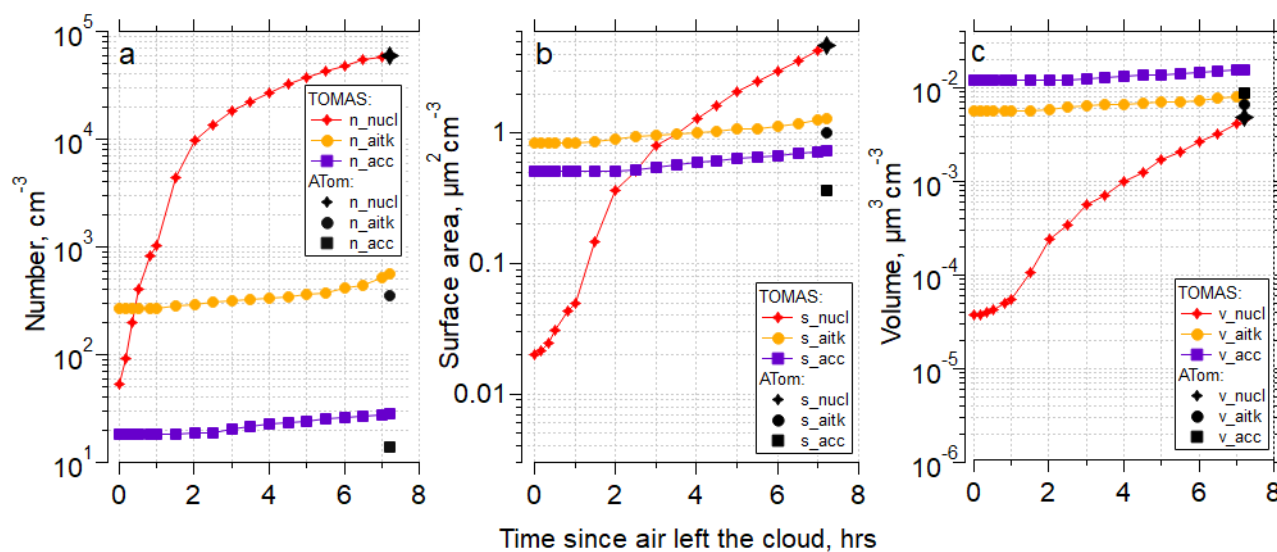
524 **Figure 6:** Results of simulations using the TOMAS box model for an example case (ATom 2, 2017-02-04, 03:05:31-03:06:30 UTC;  
 525 case identifier: sd486) where measurements were made 7.3 hours following convective influence, and temperature along the  
 526 trajectory varied between 218 and 226 K. (a) Observed (shaded bars) and simulated (lines) aerosol size distributions with best

527 normalized mean error (*NME*) calculated for  $D_p$  between 2.6 and 20 nm (blue shading) for each of the NPF and growth schemes  
 528 investigated. Best results from the MAIA box model ion-assisted + neutral binary nucleation scheme shown as a dotted black line.  
 529 (b) *NME* between the modeled and measured size distribution for the VEHK scheme with varying organics mixing ratios for  
 530 condensational growth. The color of the circle indicates the value of *NME* corresponding to a particular initial mixing ratio of SO<sub>2</sub>,  
 531 NH<sub>3</sub>, or organics that varied between 0 and 100 pptv. Blue represents the best agreement, red poorer agreement, and grey the worst  
 532 (*NME* >1). There were 64 sensitivity tests. (c) As in (b), but for the NAPA scheme. d) As in (c), but for the NAPAt scheme. (e) and  
 533 (f) as in (c) and (d) respectively, but with NH<sub>3</sub> fixed and varying organics for condensation growth. (g) as in (b) but for the RIC  
 534 scheme, which provides the lowest *NME*. There were 400 sensitivity tests for this scheme. (h) as in (b) but for the DUN scheme with  
 535 NH<sub>3</sub> set to 0 (DUN<sub>NH3=0</sub>). (i) as in (c) but for the DUN scheme. (j) as in (i) but with varying organics for condensation growth. The  
 536 table presents the *NME* results for the corresponding size distributions in panel (a) and associated initial mixing ratios of gas-phase  
 537 precursors.

538

539 Figure 7 shows the time evolution for particle number concentration, surface area, and volume for the nucleation,  
 540 Aitken, and accumulation modes using the Riccobono et al. (2014) scheme for the same case as shown in Fig. 6 for the  
 541 simulation with the lowest *NME* in Fig. 6g (SO<sub>2</sub>=1.3 pptv, organics=5.5 pptv). There is rapid evolution of the nucleation mode  
 542 and slower changes of the larger modes, and the model effectively matches the number, surface and volume of the measured  
 543 nucleation mode. In the case presented in Figure 7b, the surface area measured on ATom is dominated by the nucleation mode  
 544 particles; however, although frequent, this is not a typical pattern among all other cases studied here. In general, in the cases  
 545 with the highest surface area, values are split between nucleation, Aitken and accumulation modes almost equally (Table S5,  
 546 Fig. S68-70).

547



548

549 **Figure 7:** (a) TOMAS box model simulation of the case (case identifier: sd486) shown in Fig. 6 for the lowest (best) *NME* for the RIC  
 550 scheme, showing number concentration of the nucleation (3-12 nm), Aitken (12-60 nm) and accumulation (60-500 nm) modes as a  
 551 function of time since the air parcel exited the cloud to the time of measurement by the aircraft. Black symbols indicate values at the  
 552 point of measurement. The measured Aitken and accumulation mode values from the observations were used as approximate initial  
 553 conditions for the model simulation and are shown at time t=fin. (c) as in (a), but for surface area concentrations. (c) as in (a), but  
 554 for volume concentrations. Conditions for the simulations were diurnally varying OH concentrations with solar zenith angle. Initial  
 555 SO<sub>2</sub>=1.3 pptv, and initial organics=5.5 pptv.

556

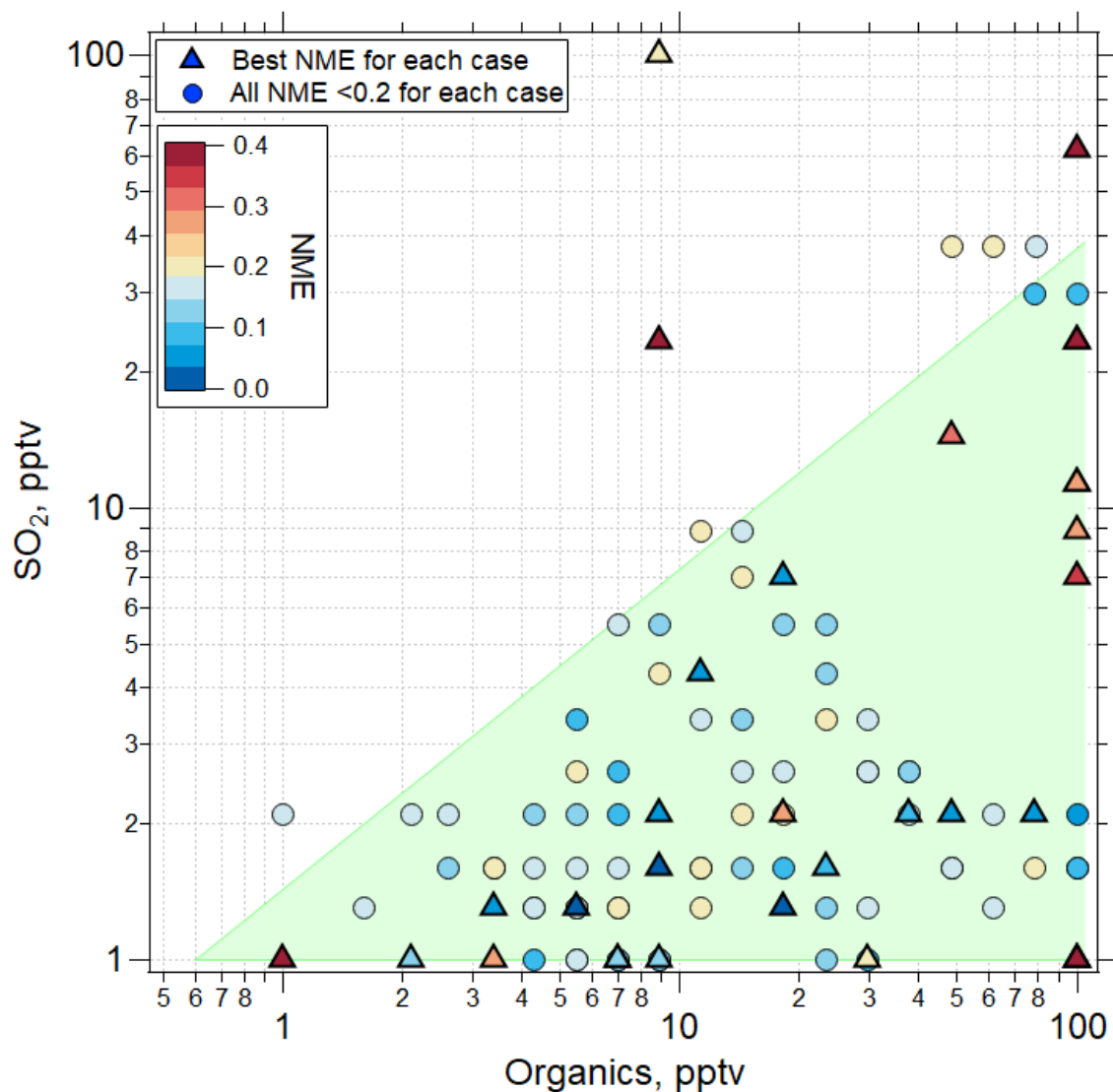
557 In 21 out of the 32 cases for which multiple box-model simulations were run, the sulfuric-acid-organic nucleation  
558 scheme of (Riccobono et al., 2014) produced lower (better) values of *NME* than the other parameterizations tested  
559 (Supplemental Material Table S4). Two of those 21 best *NME* cases for RIC were tied with NAPA and NAPAt, both with  
560 organics added for initial particle growth. The remaining 12 best *NME*s came from two different ternary nucleation schemes  
561 with added organics for growth of particles. These schemes were the NAPA or NAPAt, or the DUN with both charged and  
562 neutral channels. The majority of these ternary cases, however, required initial conditions of  $\text{NH}_3$  of 52 pptv or more, much  
563 greater than the mixing ratios expected at these locations in the UT (Höpfner et al., 2016). While we are limited by the lack of  
564 direct observations of  $\text{NH}_3$ , amines, and condensable organic species, it is plausible that there are enough of these compounds—  
565 a few to tens of pptv—to participate in ternary nucleation and subsequent growth to be consistent with the ATom measurements.  
566 Further, regardless of the available  $\text{SO}_2$ , the results strongly suggest that binary sulfuric acid-water nucleation, whether ion-  
567 assisted or neutral, and whether coupled with organic growth or not, generally cannot explain the ATom observations.

568 The findings for the case of organic-mediated NPF are summarized in Fig. 8, where we show the  $\text{SO}_2$  and organic  
569 precursor mixing ratios for all sensitivity simulations using the RIC scheme, highlighting the assumptions that yielded the  
570 lowest *NME* for each case. The results show that for all of the cases where sulfuric acid-organic nucleation most successfully  
571 simulated the observations (21 of 32 cases), initial  $\text{SO}_2$  mixing ratios  $<30$  pptv and organic precursors  $<100$  pptv (with an  
572 assumed yield of 1) were needed. These  $\text{SO}_2$  mixing ratios are consistent with observations during ATom 4 (Figs. S4, S5,  
573 Table S6) and earlier results (Rollins et al., 2017, 2018). Lacking measurements of condensable organic species, we can only  
574 speculate that a few to tens of pptv are reasonable for the marine tropical UT. Williamson et al. (2019; Extended Data Fig. 7)  
575 suggested that organics dominate the composition of smaller particles at pressure  $<400$  hPa. We note that we performed no  
576 simulations with mixing ratios of  $\text{SO}_2$  or organics above 100 pptv. While we cannot exclude that for some cases the mixing  
577 ratios of these precursors at levels above 100 pptv could improve fits, these levels are outside of prior observations so were  
578 not considered in this study.

579 In the case shown in Fig. 6, mixing ratios of  $\text{SO}_2$  and organics of  $\sim 1.3$  pptv and 5.5 pptv, respectively, were sufficient  
580 to nucleate particles and produce a size distribution that matched the observations with an *NME* of 0.02 using the RIC scheme.  
581 In a majority of the cases, the RIC scheme predicted  $\text{SO}_2 < 5$  pptv that are lower than typical UT  $\text{SO}_2$  concentrations, suggesting  
582 that our temperature extrapolation may overpredict nucleation rates at the typical  $\text{SO}_2$  mixing ratios of  $\sim 30$  pptv in the UT.  
583 Overall, the lowest *NME* values were obtained when initial  $\text{SO}_2$  values were low ( $<30$  pptv), while organics varied over a  
584 range of mixing ratios as shown by triangles in Fig. 8. This suggests that organic matter will often contribute significantly to  
585 the composition of the nucleated and growing particles on a mole basis, and even more so on a mass basis because the assumed  
586 molecular weight of organic precursors and products is  $200 \text{ g mol}^{-1}$  compared  $96 \text{ g mole}^{-1}$  for  $\text{SO}_4$ .

587

588



589  
 590  
 591  
 592  
 593  
 594  
 595  
 596

**Figure 8:** Values of *NME* (colored symbols) for best fits of the sensitivity studies. TOMAS model simulations were made using the RIC sulfuric acid-organic scheme. Among the sensitivity tests using this scheme, the one with the lowest *NME* case is shown with a triangle located at the initial conditions of SO<sub>2</sub> and organics for that case, while the next best *NME* case (provided *NME* < 0.2) is shown as a circle. The shaded region represents the approximate parameter space in which the best agreement between model and measurement is found for all the convective influence cases studied. Note a different *NME* color scale range (0 - 0.4) than the one presented in Fig. 6 (0 - 1).



598 Comparing aerosol size distribution measurements with box-model simulations shows that none of the binary neutral  
599 or ion-assisted NPF schemes are consistent with observations, regardless of precursor concentrations and the presence or  
600 absence of condensing organics for further growth. These schemes predict significant nucleation but do not make enough  
601 particles in the 5-20 nm size range (Fig.6) to match observations. Adding organics for initial growth of particles shifts the size  
602 distribution to bigger sizes but only slightly improves the model-to-measurement fits (Table S4).

603 However, schemes that incorporate organic compounds or  $\text{NH}_3$  to nucleate particles, plus condensing organics as  
604 growth agents, can plausibly replicate the observed size distributions. These results suggest that organic precursor species are  
605 likely important in NPF and initial growth in the tropical upper troposphere, even above marine regions remote from  
606 continental sources. In general, the RIC scheme provided best model-to-measurement fits; however, the improvement in the  
607 fit values for DUN scheme when organics are added for initial growth of particles suggests that organics may be more important  
608 for growth than for nucleation (Table S4).

609 We find that to best reproduce both nucleation and growth rates by the RIC scheme, the mixing ratios of gas-phase  
610 organic precursors generally needs to be at least twice that of  $\text{SO}_2$  (Fig.8). While an example in Figure 6 shows that the source  
611 of condensable organics may be even  $\sim 5$  times the  $\text{SO}_2$  mixing ratio in the remote tropical UT (Fig. S66), we do not know  
612 whether or not there may be that much more organic precursor available in this region. Although, regions where the oceanic  
613 source of SOA may be higher than the DMS source have been reported previously (e.g. Croft et al., 2019).

614 Unfortunately, we have no information on the nature and mixing ratios of oxidized organic species that participated  
615 in NPF and initial growth in this environment. The mixing ratios used in this study do not seem out of the range of possibility.  
616 Potential precursors to these condensing species, such as isoprene or monoterpenes (e.g. alpha- or beta-pinene), were found to  
617 be below the limit of instrument detection (2 pptv for isoprene, 0.1 pptv for alpha-pinene, and 0.2 pptv for beta-pinene) in the  
618 tropical UT during the ATom deployments. The exact identification of these condensing organic species would require  
619 instrumentation such as an atmospheric-pressure-interface time-of-flight (API-TOF) mass spectrometer to measure the  
620 composition of molecular clusters, which was not a part of the suite of instrumentation during the ATom mission. Other studies  
621 also suggest that NPF and growth involving organic species may be common in the remote troposphere. Willis et al. (2016)  
622 showed that marine organics contribute to the growth of newly formed particles in the summertime Arctic at low altitude;  
623 however, it was unclear if marine organics were involved in nucleation. Burkart et al. (2017) found that particle growth in the  
624 remote Arctic was largely due to condensation of unidentified organic compounds, possibly of marine origin, associated with  
625 oxidation or photochemistry of the sea-surface micro-layer (Abbatt et al., 2019). Andreae et al. (2018) proposed that oxidized  
626 biogenic VOCs were the source of recently formed particles found in the outflows and anvils of convective storms over  
627 Amazonia.

628 Chemistry-climate models rarely include organic-driven nucleation pathways in the UT where globally significant  
629 NPF takes place. This may result in poor estimates of NPF and CCN abundance and contribute to uncertainties in aerosol-

630 cloud-radiation effects. Williamson et al. (2019) showed that the production of newly formed particles and their growth to  
631 cloud-active sizes during descent towards the surface is not adequately captured in the global chemical transport models, which  
632 tend to underestimate the magnitude of tropical UT NPF and subsequent growth. This underestimate might be related to  
633 missing organic precursors, missing chemical mechanisms, or structural errors associated with convective parameterizations.  
634 According to Williamson et al. (2019), the combined direct and indirect radiative effect of NPF in the tropical UT is  $\sim 0.1 \text{ W}$   
635  $\text{m}^{-2}$ , globally.

636 The assumptions in our box model simulations point to the need for further observational and modeling studies. For  
637 example, we do not directly simulate in TOMAS the oxidation of DMS to  $\text{SO}_2$  and MSA. However, the  $\text{SO}_2$  mixing ratios  
638 estimated in this study may serve as a proxy for DMS in the modeling in our study, although the timescale for forming  $\text{H}_2\text{SO}_4$   
639 from  $\text{SO}_2$  will be incorrect. We had measurements of  $\text{SO}_2$  only during the fourth ATom deployment, and no measurements of  
640  $\text{NH}_3$  or highly oxygenated organic molecules that are likely aerosol precursors. Instead, we have constrained the box model  
641 simulations using reasonable lower and upper limits of their mixing ratios based on literature data and in case of  $\text{SO}_2$ , ATom  
642 4 data. One of the limitations of our box modeling effort is that the temperatures along the trajectories were often below the  
643 lower range limit of three (out of four) nucleation schemes evaluated (Table S6). In these cases (marked with a “\*” in  
644 Supplemental Material Figs. 15-45 and Table S6) the best-fit  $\text{SO}_2$  and organic concentrations are expected to be biased high.  
645 Although experimentally unverified, we incorporated temperature dependence into the Riccobono et al. (2014) scheme after  
646 Yu et al. (2017). We would expect faster nucleation rates at the lower trajectory temperatures than are simulated by these  
647 schemes (e.g. Yue and Hamill, 1979). Further, we have tested the Napari et al (2002) scheme both with and without a tuning  
648 factor of  $10^{-5}$  that was developed for continental regions (Jung et al., 2010; Westervelt et al., 2013), an obvious source of  
649 uncertainty when simulating NPF in the UT over the oceans. These are schemes that many models use and they do not appear  
650 to (often) work for this region, possibly due to their limited range of operating temperatures. We also have not explored the  
651 organic-only nucleation scheme described by Kirbky et al. (2016), an updated version of the Vehkamäki et al. (2002) scheme  
652 covering a wider range of temperatures and relative humidities by Maattanen et al. (2017) that has been validated against  
653 CLOUD measurements, or the recently published ternary nucleation look up tables for model implementation (Yu et al., 2020),  
654 and these schemes are worth investigating in future studies.

655 Further, we did not account for mixing with surrounding air on the path between the cloud outflow and the point of  
656 measurement when running simulations. The box model used here simulates NPF in the outflow region of deep convective  
657 clouds. Although, active NPF was identified in the vicinity of clouds and in the cloud outflow region in many studies (such as  
658 Perry and Hobbs 1994; Clarke et al., 1998, 1999; Ström et al., 1999; Clement et al., 2002; Twohy et al., 2002; Weigelt et al.,  
659 2009; Waddicor et al., 2012; de Reus et al., 2001; Clarke and Kapustin 2002; or Andreae et al., 2018), the exact location of  
660 NPF with respect to cloud remains uncertain (Kulmala et al., 2006; Waddicor et al., 2012). We assume that nucleation does  
661 not occur within the cloud, and that the outflow does not immediately mix with the surrounding air in the highly stratified  
662 upper troposphere. If NPF were to occur in a cloud or in a zone of the turbulent mixing at the cloud edge, as suggested by

663 some studies (Stroem et al., 1999; Lee et al., 2004; Weigel, 2011; Kazil et al., 2007; Kulmala et al., 2006), our results would  
664 be biased.

665 The limitations described above are important and point out the need to undertake further in situ measurements and  
666 modeling studies to confirm the suspected role of organics in UT NPF and subsequent growth in the remote troposphere. Better  
667 understanding of NPF in the remote UT, and the growth of these particles to cloud-active sizes, could substantially improve  
668 model simulations of the preindustrial atmosphere, would allow better evaluations of the effect of current anthropogenic  
669 perturbations, and could allow more confident predictions of the evolution of the climate and its response to future emission  
670 scenarios. Modeling efforts should focus on developing new nucleation mechanisms based on chamber studies conducted at  
671 temperatures more representative of the UT. Further airborne research should focus on measuring the composition of molecular  
672 clusters, sulfuric acid, organics, and NH<sub>3</sub> over the oceans and tropical continental areas. The planned Chemistry of the  
673 Atmosphere: Field Experiment in Brazil (CAFE-Brazil) study is the first expected to combine airborne measurements of  
674 nucleation-mode particle size distributions with API-TOF mass spectrometer measurements of the composition of nucleating  
675 clusters.

#### 676 **4. Summary**

677 Airborne observations during the ATom mission show a globally significant source region of newly formed particles  
678 in the tropical and subtropical UT that persists over both the Atlantic and Pacific Ocean basins over all seasons. These particles  
679 are often associated with the outflow from deep convection. Averaged across the tropics and subtropics over the Pacific, the  
680 particle number concentrations were a maximum (reaching as high as ~40,000 cm<sup>-3</sup>) at altitudes above 10 km where the  
681 condensation sink from pre-existing aerosol particles was a minimum. Using back-trajectories to identify convectively  
682 influenced air parcels, the highest concentrations of recently formed particles were generally found where the CI was most  
683 recent, particularly during the first and second ATom deployments. The number concentration of nucleation-mode particles  
684 decreased with time since CI due to the effects of coagulation and condensational growth. During ATom 1 and 2, particle size  
685 increased with time since CI, showing clear evidence for this growth.

686 We simulated particle nucleation and growth using two box models constrained to follow the calculated trajectories  
687 from the point of convective detrainment to the point of measurement by the aircraft, and we performed sensitivity tests varying  
688 the nucleation mechanisms and initial conditions such as precursor (SO<sub>2</sub>, NH<sub>3</sub>, organics), OH, and pre-existing particle  
689 concentrations.

690 These simulations indicate that nucleation schemes commonly used in global models, such as binary homogeneous  
691 H<sub>2</sub>SO<sub>4</sub> (both neutral by Vehkamäki et al. (2002) or ternary H<sub>2</sub>SO<sub>4</sub>+ NH<sub>3</sub> (neutral with and without a tuning factor by Napari  
692 et al. (2002) and Jung et al. (2010)), as well as the recently developed neutral and ion-induced binary and ternary nucleation  
693 scheme by Dunne et al. (2016), were all inconsistent with observed size distributions in all simulated cases when no organics  
694 were included for growth. This result also held for the binary nucleation mechanisms even when organics were added as a

695 condensing, but not nucleating, species. Adding organics for initial growth of particles formed by either of tested ternary  
696 schemes (Napari et al. (2002) or Dunne et al. (2016)) provided the best fits in 12 out of 32 simulated cases (Table S4). However,  
697 the majority of these ternary inorganic simulations required initial conditions of  $\text{NH}_3 > 50$  pptv, which is substantially greater  
698 than expected at these locations in the UT (Höpfner et al., 2016).

699 In contrast, a scheme involving oxidation products of biogenic organics and  $\text{H}_2\text{SO}_4$  (Riccobono et al., 2014) gave  
700 results that were most consistent among the various models with observations in 21 out of 32 cases, while in 2 cases it was  
701 tied for the lowest NME with other schemes. These results strongly suggest that organics are involved in NPF and subsequent  
702 initial growth in the remote tropical UT. This supports the finding by Simon et al (2019) that organics, despite their lower  
703 oxidation level and yield at low temperatures, may be important for nucleation and growth in the UT. However, the predicted  
704  $\text{SO}_2$  concentrations were often anomalously low ( $< 5$  pptv), suggesting that our temperature extrapolation may overestimate  
705 the nucleation rates. While the Riccobono scheme was most consistent, the analysis suggests that multiple nucleation  
706 mechanisms may be plausible across the 32 cases.

707 We have assumed that the Riccobono et al. (2014) scheme, which was developed from laboratory measurements of  
708 nucleation from the oxidation products of terrestrial biogenic VOCs, represents processes in the remote marine UT of the  
709 tropical Pacific. In fact, there is virtually no information on the nature of oxidized organic species (or ammonia and amines)  
710 that may participate in NPF in this environment. Also, the Riccobono scheme, one of the least constrained nucleation  
711 mechanisms, required a large extrapolation in temperature to simulate UT conditions. Given that NPF in the tropical UT is a  
712 major source of CCN over a large portion of the globe (Williamson et al., 2019), we recommend that future work investigate  
713 the species contributing to NPF and growth explicitly, including direct measurements when possible. Additionally, we  
714 recommend studies that focus on potential tropical marine sources of aerosol precursor gases, the efficiency of their transport  
715 to the UT, the products of their oxidation, and the mechanisms of NPF at temperatures  $< 230$  K.

## 716 **Data availability**

717 The full ATom dataset is available as given in Wofsy et al. (2018), and may also be accessed at  
718 <https://espoarchive.nasa.gov/archive/browse/atom>. Data presented in this analysis are available at the Oak Ridge National  
719 Laboratory (ORNL) Distributed Active Archive Center, (DAAC) Kupc et al. (2020).

## 720 **Author contributions**

721 AK, CW, CB, KF, MD, BW, TB, AR collected data. AK, JP, CB, and AH conceived and designed the study. AK performed  
722 the analysis and wrote the manuscript with help from CB and JP, with contributions from all co-authors. JP, AH, JK provided  
723 TOMAS and MAIA box models and helped with model upgrades. AK performed all model simulations. MD and BW analysed  
724 cloud properties. ER calculated the air parcel back-trajectories.

725 **Competing interests**

726 The authors declare that they have no conflicts of interest.

727 **Disclaimer**

728 The contents do not necessarily represent the official views of the University of Colorado, the University of Vienna, NOAA  
729 or of the respective granting agencies. The use or mention of commercial products or services does not represent an  
730 endorsement by the authors or by any agency.

731 **Acknowledgements**

732 We thank Ken Aikin for contributions to this analysis, and the ATom science team and NASA DC-8 flight crew for their  
733 contributions to the ATom data. We are grateful for the hard work of the ATom leadership and logistics teams. We thank the  
734 Whole Air Sampler (WAS; UCI) and the Trace Organic Gas Analyzer (TOGA; NCAR) teams for access to their data.

735 **Financial Statement**

736 This work was funded by NASA's Earth System Science Pathfinder Program under award NNH15AB12I and by NOAA's  
737 Health of the Atmosphere and Atmospheric Chemistry, Carbon Cycle, and Climate Programs. Agnieszka Kupc was supported  
738 by the Austrian Science Fund FWF's Erwin Schrodinger Fellowship J-3613. Bernadett Weinzierl and Maximilian Dollner  
739 were supported by European Research Council (ERC) under the European Union's Horizon 2020 research and innovation  
740 framework program under grant 640458 (A-LIFE) and by the University of Vienna. Jeffrey Pierce and Anna Hodshire were  
741 supported by the US Department of Energy's Atmospheric System Research, an Office of Science, Office of Biological and  
742 Environmental Research program, under grant DE-SC0019000; and the NOAA, Office of Science, Office of Atmospheric  
743 Chemistry, Carbon Cycle, and Climate Program, under cooperative agreement award NA17OAR430001.

744

745 **References**

746

747 Abbatt, J. P. D., Leaitch, W. R., Aliabadi, A. A., Bertram, A. K., Blanchet, J. P., Boivin-Rioux, A., Bozem,  
748 H., Burkart, J., Chang, R. Y. W., Charette, J., Chaubey, J. P., Christensen, R. J., Cirisan, A., Collins,  
749 D. B., Croft, B., Dionne, J., Evans, G. J., Fletcher, C. G., Galí, M., Ghahremaninezhad, R., Girard, E.,  
750 Gong, W., Gosselin, M., Gourdal, M., Hanna, S. J., Hayashida, H., Herber, A. B., Hesaraki, S., Hoor,  
751 P., Huang, L., Hussherr, R., Irish, V. E., Keita, S. A., Kodros, J. K., Köllner, F., Kolonjari, F., Kunkel,  
752 D., Ladino, L. A., Law, K., Lévassieur, M., Libois, Q., Liggio, J., Lizotte, M., Macdonald, K. M.,

- 753 Mahmood, R., Martin, R. V., Mason, R. H., Miller, L. A., Moravek, A., Mortenson, E., Mungall, E.  
754 L., Murphy, J. G., Namazi, M., Norman, A. L., O'Neill, N. T., Pierce, J. R., Russell, L. M., Schneider,  
755 J., Schulz, H., Sharma, S., Si, M., Staebler, R. M., Steiner, N. S., Thomas, J. L., von Salzen, K.,  
756 Wentzell, J. J. B., Willis, M. D., Wentworth, G. R., Xu, J. W., and Yakobi-Hancock, J. D.: Overview  
757 paper: New insights into aerosol and climate in the Arctic, *Atmos. Chem. Phys.*, 19, 2527-2560,  
758 10.5194/acp-19-2527-2019, 2019.
- 759 Adams, P. J., Seinfeld, J. H., and Koch, D. M.: Global concentrations of tropospheric sulfate, nitrate, and  
760 ammonium aerosol simulated in a general circulation model, *J. Geophys. Res.*, 104, 13791-13823,  
761 10.1029/1999jd900083, 1999.
- 762 Adams, P. J., and Seinfeld, J. H.: Predicting global aerosol size distributions in general circulation models, *J.*  
763 *Geophys. Res.*, 107, AAC 4-1-AAC 4-23, 10.1029/2001jd001010, 2002.
- 764 Almeida, J., Schobesberger, S., Kürten, A., Ortega, I. K., Kupiainen-Määttä, O., Praplan, A. P., Adamov, A.,  
765 Amorim, A., Bianchi, F., Breitenlechner, M., David, A., Dommen, J., Donahue, N. M., Downard, A.,  
766 Dunne, E., Duplissy, J., Ehrhart, S., Flagan, R. C., Franchin, A., Guida, R., Hakala, J., Hansel, A.,  
767 Heinritzi, M., Henschel, H., Jokinen, T., Junninen, H., Kajos, M., Kangasluoma, J., Keskinen, H.,  
768 Kupc, A., Kurtén, T., Kvashin, A. N., Laaksonen, A., Lehtipalo, K., Leiminger, M., Leppä, J.,  
769 Loukonen, V., Makhmutov, V., Mathot, S., McGrath, M. J., Nieminen, T., Olenius, T., Onnela, A.,  
770 Petäjä, T., Riccobono, F., Riipinen, I., Rissanen, M., Rondo, L., Ruuskanen, T., Santos, F. D., Sarnela,  
771 N., Schallhart, S., Schnitzhofer, R., Seinfeld, J. H., Simon, M., Sipilä, M., Stozhkov, Y., Stratmann,  
772 F., Tomé, A., Tröstl, J., Tsagkogeorgas, G., Vaattovaara, P., Viisanen, Y., Virtanen, A., Vrtala, A.,  
773 Wagner, P. E., Weingartner, E., Wex, H., Williamson, C., Wimmer, D., Ye, P., Yli-Juuti, T., Carslaw,  
774 K. S., Kulmala, M., Curtius, J., Baltensperger, U., Worsnop, D. R., Vehkamäki, H., and Kirkby, J.:  
775 Molecular understanding of sulphuric acid–amine particle nucleation in the atmosphere, *Nature*, 502,  
776 359, 10.1038/nature12663, 2013.
- 777 Andreae, M. O., Afchine, A., Albrecht, R., Holanda, B. A., Artaxo, P., Barbosa, H. M. J., Borrmann, S.,  
778 Cecchini, M. A., Costa, A., Dollner, M., Fütterer, D., Järvinen, E., Jurkat, T., Klimach, T., Konemann,  
779 T., Knote, C., Krämer, M., Krisna, T., Machado, L. A. T., Mertes, S., Minikin, A., Pöhlker, C.,  
780 Pöhlker, M. L., Pöschl, U., Rosenfeld, D., Sauer, D., Schlager, H., Schnaiter, M., Schneider, J., Schulz,  
781 C., Spanu, A., Sperling, V. B., Voigt, C., Walser, A., Wang, J., Weinzierl, B., Wendisch, M., and  
782 Ziereis, H.: Aerosol characteristics and particle production in the upper troposphere over the Amazon  
783 Basin, *Atmos. Chem. Phys.*, 18, 921-961, 10.5194/acp-18-921-2018, 2018.
- 784 Atkinson, R., and Arey, J.: Atmospheric degradation of volatile organic compounds, *Chemical Reviews*, 103,  
785 4605-4638, 10.1021/cr0206420, 2003.
- 786 Bianchi, F., Tröstl, J., Junninen, H., Frege, C., Henne, S., Hoyle, C. R., Molteni, U., Herrmann, E., Adamov,  
787 A., Bukowiecki, N., Chen, X., Duplissy, J., Gysel, M., Hutterli, M., Kangasluoma, J., Kontkanen, J.,  
788 Kürten, A., Manninen, H. E., Münch, S., Peräkylä, O., Petäjä, T., Rondo, L., Williamson, C.,  
789 Weingartner, E., Curtius, J., Worsnop, D. R., Kulmala, M., Dommen, J., and Baltensperger, U.: New  
790 particle formation in the free troposphere: A question of chemistry and timing, *Science*, 352, 1109-  
791 1112, 10.1126/science.aad5456, 2016.
- 792 Bork, N., Elm, J., Olenius, T., and Vehkamäki, H.: Methane sulfonic acid-enhanced formation of molecular  
793 clusters of sulfuric acid and dimethyl amine, *Atmos. Chem. Phys.*, 14, 12023–12030,  
794 <https://doi.org/10.5194/acp-14-12023-2014>, 2014.
- 795 Borrmann, S., Kunkel, D., Weigel, R., Minikin, A., Deshler, T., Wilson, J. C., Curtius, J., Volk, C. M., Homan,  
796 C. D., Ulanovsky, A., Ravegnani, F., Viciani, S., Shur, G. N., Belyaev, G. V., Law, K. S., and Cairo,  
797 F.: Aerosols in the tropical and subtropical UT/LS: in-situ measurements of submicron particle  
798 abundance and volatility, *Atmos. Chem. Phys.*, 10, 5573-5592, 10.5194/acp-10-5573-2010, 2010.

- 799 Bowman, K. P.: Large-scale isentropic mixing properties of the Antarctic polar vortex from analyzed winds,  
800 *J. Geophys. Res.*, 98, 23013-23027, 10.1029/93jd02599, 1993.
- 801 Brock, C. A., Hamill, P., Wilson, J. C., Jonsson, H. H., and Chan, K. R.: Particle formation in the upper tropical  
802 troposphere: A source of nuclei for the stratospheric aerosol, *Science*, 270, 1650-1653,  
803 10.1126/science.270.5242.1650, 1995.
- 804 Brock, C. A., Williamson, C., Kupc, A., Froyd, K. D., Erdesz, F., Wagner, N., Richardson, M., Schwarz, J.  
805 P., Gao, R. S., Katich, J. M., Campuzano-Jost, P., Nault, B. A., Schroder, J. C., Jimenez, J. L.,  
806 Weinzierl, B., Dollner, M., Bui, T., and Murphy, D. M.: Aerosol size distributions during the  
807 Atmospheric Tomography Mission (ATom): methods, uncertainties, and data products, *Atmos. Meas.*  
808 *Tech.*, 12, 3081-3099, 10.5194/amt-12-3081-2019, 2019.
- 809 Brune, W. H., Miller, D. O., Thames, A. B., Allen, H. M., Apel, E. C., Blake, D. R., et al.: Exploring oxidation  
810 in the remote free troposphere: Insights from Atmospheric Tomography (ATom), *Geophys. Res:*  
811 *Atmos*, 125, e2019JD031685. <https://doi.org/10.1029/2019JD031685>, 2020
- 812 Burkart, J., Hodshire, A. L., Mungall, E. L., Pierce, J. R., Collins, D. B., Ladino, L. A., Lee, A. K. Y., Irish,  
813 V., Wentzell, J. J. B., Liggio, J., Papakyriakou, T., Murphy, J., and Abbatt, J.: Organic condensation  
814 and particle growth to CCN sizes in the summertime marine Arctic is driven by materials more  
815 semivolatile than at continental sites, *Geophys. Res. Lett.*, 44, 725-710,734,  
816 10.1002/2017gl075671, 2017.
- 817 Chen, H., Karion, A., Rella, C. W., Winderlich, J., Gerbig, C., Filges, A., Newberger, T., Sweeney, C., and  
818 Tans, P. P.: Accurate measurements of carbon monoxide in humid air using the cavity ring-down  
819 spectroscopy (CRDS) technique, *Atmos. Meas. Tech.*, 6, 1031–1040, [https://doi.org/10.5194/amt-6-](https://doi.org/10.5194/amt-6-1031-2013)  
820 [1031-2013](https://doi.org/10.5194/amt-6-1031-2013), 2013
- 821 Chen, H., Ezell, M. J., Arquero, K. D., Varner, M. E., Dawson, M. L., Gerber, R. B., and Finlayson-Pitts, B.  
822 J.: New particle formation and growth from methanesulfonic acid, trimethylamine and water, *Phys.*  
823 *Chem. Chem. Phys.*, 17, 13699–13709, <https://doi.org/10.1039/c5cp00838g>, 2015.
- 824 Chen, H. and Finlayson-Pitts, B. J.: New particle formation from methanesulfonic acid and amines/ammonia  
825 as a function of temperature, *Environ. Sci. Technol.*, 51, 243–252,  
826 <https://doi.org/10.1021/acs.est.6b04173>, 2017.
- 827 Clarke, A. D.: Atmospheric nuclei in the remote free-troposphere, *J. Atmos. Chem.*, 14, 479-488,  
828 10.1007/BF00115252, 1992.
- 829 Clarke, A. D.: Atmospheric nuclei in the Pacific midtroposphere: Their nature, concentration, and evolution,  
830 *J. Geophys. Res.*, 98, 20633-20647, 10.1029/93jd00797, 1993.
- 831 Clarke, A. D., Davis, D., Kapustin, V. N., Eisele, F., Chen, G., Paluch, I., Lenschow, D., Bandy, A. R.,  
832 Thornton, D., Moore, K., Mauldin, L., Tanner, D., Litchy, M., Carroll, M. A., Collins, J., and  
833 Albercook, G.: Particle Nucleation in the Tropical Boundary Layer and Its Coupling to Marine Sulfur  
834 Sources, *Science*, 282, 89-92, 10.1126/science.282.5386.89, 1998.
- 835 Clarke, A. D., F. Eisele, V. N. Kapustin, K. Moore, D. Tanner, L. Mauldin, M. Litchy, B. Lienert, M. A.  
836 Carroll, and G. Albercook, Nucleation in the equatorial free troposphere: Favorable environments  
837 during PEM-Tropics, *J. Geophys. Res.*, 104, 5735–5744, 1999.
- 838 Clarke, A. D., and Kapustin, V. N.: A Pacific Aerosol Survey. Part I: A Decade of Data on Particle Production,  
839 Transport, Evolution, and Mixing in the Troposphere, *Journal of J. Atmos. Sci.*, 59, 363-382,  
840 10.1175/1520-0469(2002)059<0363:Apaspi>2.0.Co;2, 2002.
- 841 Clarke, A. D., S. R. Owens, and J. Zhou , An ultrafine sea-salt flux from breaking waves: Implications for  
842 cloud condensation nuclei in the remote marine atmosphere, *J. Geophys. Res.*, 111, D06202,  
843 doi:10.1029/2005JD006565, 2006

- 844 Clement, C. F., I. J. Ford, C. H. Twohy, A. J. Weinheimer, and T. Campos, Particle production in the outflow  
845 of a mid-latitude storm, *J. Geophys. Res.*, 10.1029/2001JD001352, 2002.
- 846 Croft, B., Martin, R. V., Leaitch, W. R., Burkart, J., Chang, R. Y.-W., Collins, D. B., Hayes, P. L., Hodshire,  
847 A. L., Huang, L., Kodros, J. K., Moravek, A., Mungall, E. L., Murphy, J. G., Sharma, S., Tremblay,  
848 S., Wentworth, G. R., Willis, M. D., Abbatt, J. P. D., and Pierce, J. R.: Arctic marine secondary organic  
849 aerosol contributes significantly to summertime particle size distributions in the Canadian Arctic  
850 Archipelago, *Atmos. Chem. Phys.*, 19, 2787–2812, <https://doi.org/10.5194/acp-19-2787-2019>, 2019.
- 851 de Reus, M., R. Krejci, R. Scheele, J. Williams, H. Fischer, and J. Ström, Vertical distributions of the aerosol  
852 number concentration and size distribution over the northern hemisphere Indian Ocean, *J. Geophys.*  
853 *Res.*, 106, 28,629–28,642, 2001.
- 854 Dunne, E. M., Gordon, H., Kürten, A., Almeida, J., Duplissy, J., Williamson, C., Ortega, I. K., Pringle, K. J.,  
855 Adamov, A., Baltensperger, U., Barmet, P., Benduhn, F., Bianchi, F., Breitenlechner, M., Clarke, A.,  
856 Curtius, J., Dommen, J., Donahue, N. M., Ehrhart, S., Flagan, R. C., Franchin, A., Guida, R., Hakala,  
857 J., Hansel, A., Heinritzi, M., Jokinen, T., Kangasluoma, J., Kirkby, J., Kulmala, M., Kupc, A., Lawler,  
858 M. J., Lehtipalo, K., Makhmutov, V., Mann, G., Mathot, S., Merikanto, J., Miettinen, P., Nenes, A.,  
859 Onnela, A., Rap, A., Reddington, C. L. S., Riccobono, F., Richards, N. A. D., Rissanen, M. P., Rondo,  
860 L., Sarnela, N., Schobesberger, S., Sengupta, K., Simon, M., Sipilä, M., Smith, J. N., Stozkhov, Y.,  
861 Tomé, A., Tröstl, J., Wagner, P. E., Wimmer, D., Winkler, P. M., Worsnop, D. R., and Carslaw, K.  
862 S.: Global atmospheric particle formation from CERN CLOUD measurements, *Science*, 354, 1119-  
863 1124, 10.1126/science.aaf2649, 2016.
- 864 English, J. M., Toon, O. B., Mills, M. J., and Yu, F.: Microphysical simulations of new particle formation in  
865 the upper troposphere and lower stratosphere, *Atmos. Chem. Phys.*, 11, 9303-9322, 10.5194/acp-11-  
866 9303-2011, 2011.
- 867 Faloon, I. C., Tan, D., Leshner, R. L., Hazen, N. L., Frame, C. L., Simpas, J. B., Harder, H., Martinez, M., Di  
868 Carlo, P., Ren, X., and Brune, W. H.: A laser-induced fluorescence instrument for detecting  
869 tropospheric OH and HO<sub>2</sub>: Characteristics and calibration, *J. Atmos. Chem.*, 47, 139-167,  
870 10.1023/B:JOCH.0000021036.53185.0e, 2004.
- 871 Feng, Y., and Penner, J. E.: Global modeling of nitrate and ammonium: Interaction of aerosols and  
872 tropospheric chemistry, *J. Geophys. Res.*, 112, 10.1029/2005jd006404, 2007.
- 873 Froyd, K. D., Murphy, D. M., Sanford, T. J., Thomson, D. S., Wilson, J. C., Pfister, L., and Lait, L.: Aerosol  
874 composition of the tropical upper troposphere, *Atmos. Chem. Phys.*, 9, 4363-4385, 10.5194/acp-9-  
875 4363-2009, 2009.
- 876 Froyd, K. D., Murphy, D. M., Brock, C. A., Campuzano-Jost, P., Dibb, J. E., Jimenez, J.-L., Kupc, A.,  
877 Middlebrook, A. M., Schill, G. P., Thornhill, K. L., Williamson, C. J., Wilson, J. C., and Ziemba, L.  
878 D.: A new method to quantify mineral dust and other aerosol species from aircraft platforms using  
879 single-particle mass spectrometry, *Atmos. Meas. Tech.*, 12, 6209–6239, <https://doi.org/10.5194/amt-12-6209-2019>, 2019.
- 881 Gao, R. S., Rosenlof, K. H., Fahey, D. W., Wennberg, P. O., Hintsala, E. J., and Hanisco, T. F.: OH in the  
882 tropical upper troposphere and its relationships to solar radiation and reactive nitrogen, *J. Atmos.*  
883 *Chem.*, 71, 55-64, 10.1007/s10874-014-9280-2, 2014.
- 884 Gordon, H., Sengupta, K., Rap, A., Duplissy, J., Frege, C., Williamson, C., Heinritzi, M., Simon, M., Yan, C.,  
885 Almeida, J., Tröstl, J., Nieminen, T., Ortega, I. K., Wagner, R., Dunne, E. M., Adamov, A., Amorim,  
886 A., Bernhammer, A.-K., Bianchi, F., Breitenlechner, M., Brilke, S., Chen, X., Craven, J. S., Dias, A.,  
887 Ehrhart, S., Fischer, L., Flagan, R. C., Franchin, A., Fuchs, C., Guida, R., Hakala, J., Hoyle, C. R.,  
888 Jokinen, T., Junninen, H., Kangasluoma, J., Kim, J., Kirkby, J., Krapf, M., Kürten, A., Laaksonen, A.,  
889 Lehtipalo, K., Makhmutov, V., Mathot, S., Molteni, U., Monks, S. A., Onnela, A., Peräkylä, O., Piel,



- 890 F., Petäjä, T., Praplan, A. P., Pringle, K. J., Richards, N. A. D., Rissanen, M. P., Rondo, L., Sarnela,  
891 N., Schobesberger, S., Scott, C. E., Seinfeld, J. H., Sharma, S., Sipilä, M., Steiner, G., Stozhkov, Y.,  
892 Stratmann, F., Tomé, A., Virtanen, A., Vogel, A. L., Wagner, A. C., Wagner, P. E., Weingartner, E.,  
893 Wimmer, D., Winkler, P. M., Ye, P., Zhang, X., Hansel, A., Dommen, J., Donahue, N. M., Worsnop,  
894 D. R., Baltensperger, U., Kulmala, M., Curtius, J., and Carslaw, K. S.: Reduced anthropogenic aerosol  
895 radiative forcing caused by biogenic new particle formation, *Proc. Nat. Acad. Sci.*, 113, 12053-12058,  
896 10.1073/pnas.1602360113, 2016.
- 897 Gordon, H., Kirkby, J., Baltensperger, U., Bianchi, F., Breitenlechner, M., Curtius, J., Dias, A., Dommen, J.,  
898 Donahue, N. M., Dunne, E. M., Duplissy, J., Ehrhart, S., Flagan, R. C., Frege, C., Fuchs, C., Hansel,  
899 A., Hoyle, C. R., Kulmala, M., Kürten, A., Lehtipalo, K., Makhmutov, V., Molteni, U., Rissanen, M.  
900 P., Stozhkov, Y., Tröstl, J., Tsagkogeorgas, G., Wagner, R., Williamson, C., Wimmer, D., Winkler,  
901 P. M., Yan, C., and Carslaw, K. S.: Causes and importance of new particle formation in the present-  
902 day and preindustrial atmospheres, *J. Geophys. Res.*, 122, 8739-8760, 10.1002/2017jd026844, 2017.
- 903 Hodshire, A. L., Palm, B. B., Alexander, M. L., Bian, Q., Campuzano-Jost, P., Cross, E. S., Day, D. A., de Sá,  
904 S. S., Guenther, A. B., Hansel, A., Hunter, J. F., Jud, W., Karl, T., Kim, S., Kroll, J. H., Park, J. H.,  
905 Peng, Z., Seco, R., Smith, J. N., Jimenez, J. L., and Pierce, J. R.: Constraining nucleation,  
906 condensation, and chemistry in oxidation flow reactors using size-distribution measurements and  
907 aerosol microphysical modeling, *Atmos. Chem. Phys.*, 18, 12433-12460, 10.5194/acp-18-12433-  
908 2018, 2018.
- 909 Hodshire, A. L., Bian, Q., Ramnarine, E., Lonsdale, C. R., Alvarado, M. J., Kreidenweis, S. M., et al. (2019).  
910 More than emissions and chemistry: Fire size, dilution, and background aerosol also greatly influence  
911 near-field biomass burning aerosol aging. *J. Geophys. Res.: Atmos.*, 124, 5589–5611. [https://doi.org/  
912 10.1029/2018JD029674](https://doi.org/10.1029/2018JD029674), 2019.
- 913 Höpfner, M., Volkamer, R., Grabowski, U., Grutter, M., Orphal, J., Stiller, G., von Clarmann, T., and Wetzel,  
914 G.: First detection of ammonia (NH<sub>3</sub>) in the Asian summer monsoon upper troposphere, *Atmos.*  
915 *Chem. Phys.*, 16, 14357-14369, 10.5194/acp-16-14357-2016, 2016.
- 916 IPCC: Climate Change 2013: The Physical Science Basis. Contribution of Working Group I to the Fifth  
917 Assessment Report of the Intergovernmental Panel on Climate Change, Cambridge University Press,  
918 Cambridge, United Kingdom and New York, NY, USA, 1535 pp., 2013.
- 919 Jen, C. N., Zhao, J., McMurry, P. H., and Hanson, D. R.: Chemical ionization of clusters formed from sulfuric  
920 acid and dimethylamine or diamines, *Atmos. Chem. Phys.*, 16, 12513-12529, 10.5194/acp-16-12513-  
921 2016, 2016.
- 922 Jung, J., Fountoukis, C., Adams, P. J., and Pandis, S. N.: Simulation of in situ ultrafine particle formation in  
923 the eastern United States using PMCAMx-UF, *J. Geophys. Res.*, 115, 10.1029/2009jd012313, 2010.
- 924 Kazil, J., and Lovejoy, E. R.: A semi-analytical method for calculating rates of new sulfate aerosol formation  
925 from the gas phase, *Atmos. Chem. Phys.*, 7, 3447-3459, 10.5194/acp-7-3447-2007, 2007.
- 926 Kazil, J., Stier, P., Zhang, K., Quaas, J., Kinne, S., O'Donnell, D., Rast, S., Esch, M., Ferrachat, S., Lohmann,  
927 U., and Feichter, J.: Aerosol nucleation and its role for clouds and Earth's radiative forcing in the  
928 aerosol-climate model ECHAM5-HAM, *Atmos. Chem. Phys.*, 10, 10733–10752,  
929 <https://doi.org/10.5194/acp-10-10733-2010>, 2010
- 930 Kerminen, V.-M., Chen, X., Vakkari, V., Petäjä, T., Kulmala, M., and Bianchi, F.: Atmospheric new particle  
931 formation and growth: review of field observations, *Environ. Res. Lett.*, 13, 103003, 10.1088/1748-  
932 9326/aadf3c, 2018.
- 933 Kirkby, J., Curtius, J., Almeida, J., Dunne, E., Duplissy, J., Ehrhart, S., Franchin, A., Gagné, S., Ickes, L.,  
934 Kürten, A., Kupc, A., Metzger, A., Riccobono, F., Rondo, L., Schobesberger, S., Tsagkogeorgas, G.,  
935 Wimmer, D., Amorim, A., Bianchi, F., Breitenlechner, M., David, A., Dommen, J., Downard, A.,

936 Ehn, M., Flagan, R. C., Haider, S., Hansel, A., Hauser, D., Jud, W., Junninen, H., Kreissl, F., Kvashin,  
937 A., Laaksonen, A., Lehtipalo, K., Lima, J., Lovejoy, E. R., Makhmutov, V., Mathot, S., Mikkilä, J.,  
938 Minginette, P., Mogo, S., Nieminen, T., Onnela, A., Pereira, P., Petäjä, T., Schnitzhofer, R., Seinfeld,  
939 J. H., Sipilä, M., Stozhkov, Y., Stratmann, F., Tomé, A., Vanhanen, J., Viisanen, Y., Vrtala, A.,  
940 Wagner, P. E., Walther, H., Weingartner, E., Wex, H., Winkler, P. M., Carslaw, K. S., Worsnop, D.  
941 R., Baltensperger, U., and Kulmala, M.: Role of sulphuric acid, ammonia and galactic cosmic rays in  
942 atmospheric aerosol nucleation, *Nature*, 476, 429-433, 10.1038/nature10343, 2011.

943 Kirkby, J., Duplissy, J., Sengupta, K., Frege, C., Gordon, H., Williamson, C., Heinritzi, M., Simon, M., Yan,  
944 C., Almeida, J., Tröstl, J., Nieminen, T., Ortega, I. K., Wagner, R., Adamov, A., Amorim, A.,  
945 Bernhammer, A.-K., Bianchi, F., Breitenlechner, M., Brilke, S., Chen, X., Craven, J., Dias, A.,  
946 Ehrhart, S., Flagan, R. C., Franchin, A., Fuchs, C., Guida, R., Hakala, J., Hoyle, C. R., Jokinen, T.,  
947 Junninen, H., Kangasluoma, J., Kim, J., Krapf, M., Kürten, A., Laaksonen, A., Lehtipalo, K.,  
948 Makhmutov, V., Mathot, S., Molteni, U., Onnela, A., Peräkylä, O., Piel, F., Petäjä, T., Praplan, A. P.,  
949 Pringle, K., Rap, A., Richards, N. A. D., Riipinen, I., Rissanen, M. P., Rondo, L., Sarnela, N.,  
950 Schobesberger, S., Scott, C. E., Seinfeld, J. H., Sipilä, M., Steiner, G., Stozhkov, Y., Stratmann, F.,  
951 Tomé, A., Virtanen, A., Vogel, A. L., Wagner, A. C., Wagner, P. E., Weingartner, E., Wimmer, D.,  
952 Winkler, P. M., Ye, P., Zhang, X., Hansel, A., Dommen, J., Donahue, N. M., Worsnop, D. R.,  
953 Baltensperger, U., Kulmala, M., Carslaw, K. S., and Curtius, J.: Ion-induced nucleation of pure  
954 biogenic particles, *Nature*, 533, 521, 10.1038/nature17953, 2016.

955 Kulmala, M., Lehtinen, K. E. J., and Laaksonen, A.: Cluster activation theory as an explanation of the linear  
956 dependence between formation rate of 3nm particles and sulphuric acid concentration, *Atmos. Chem.*  
957 *Phys.*, 6, 787-793, 10.5194/acp-6-787-2006, 2006.

958 Kulmala, M., Kontkanen, J., Junninen, H., Lehtipalo, K., Manninen, H. E., Nieminen, T., Petäjä, T., Sipilä,  
959 M., Schobesberger, S., Rantala, P., Franchin, A., Jokinen, T., Järvinen, E., Äijälä, M., Kangasluoma,  
960 J., Hakala, J., Aalto, P. P., Paasonen, P., Mikkilä, J., Vanhanen, J., Aalto, J., Hakola, H., Makkonen,  
961 U., Ruuskanen, T., Mauldin, R. L., Duplissy, J., Vehkamäki, H., Bäck, J., Kortelainen, A., Riipinen,  
962 I., Kurtén, T., Johnston, M. V., Smith, J. N., Ehn, M., Mentel, T. F., Lehtinen, K. E. J., Laaksonen,  
963 A., Kerminen, V.-M., and Worsnop, D. R.: Direct observations of atmospheric aerosol nucleation,  
964 *Science*, 339, 943-946, 10.1126/science.1227385, 2013.

965 Kulmala, M., Petäjä, T., Ehn, M., Thornton, J., Sipilä, M., Worsnop, D. R., and Kerminen, V.-M.: Chemistry  
966 of Atmospheric Nucleation: On the recent advances on precursor characterization and atmospheric  
967 cluster composition in connection with atmospheric new particle formation, *Ann. Rev. Phys. Chem.*,  
968 65, 21-37, 10.1146/annurev-physchem-040412-110014, 2014.

969 Kupc, A., Williamson, C., Wagner, N. L., Richardson, M., and Brock, C. A.: Modification, calibration, and  
970 performance of the Ultra-High Sensitivity Aerosol Spectrometer for particle size distribution and  
971 volatility measurements during the Atmospheric Tomography Mission (ATom) airborne campaign,  
972 *Atmos. Meas. Tech.*, 11, 369-383, 10.5194/amt-11-369-2018, 2018.

973 Kupc, A., Williamson, C. J., Hodshire, A. L., Kazil, J., Ray, E., Brune, W. H., Bui, T. P., Dollner, M., Froyd,  
974 K. D., McKain, K., Murphy D. M., Rollins, A., Schill, G. P., Sweeny C., Thames, A., Weinzierl B.  
975 B., Pierce, J. R., and Brock, C. A.: ATom: Investigating species that control new particle formation  
976 and initial growth, Oak Ridge, Tennessee, USA: ORNL DAAC:  
977 <https://doi.org/10.3334/ORNLDAAC/1811>, 2020.

978 Kürten, A., Bianchi, F., Almeida, J., Kupiainen-Määttä, O., Dunne, E. M., Duplissy, J., Williamson, C.,  
979 Barmet, P., Breitenlechner, M., Dommen, J., Donahue, N. M., Flagan, R. C., Franchin, A., Gordon,  
980 H., Hakala, J., Hansel, A., Heinritzi, M., Ickes, L., Jokinen, T., Kangasluoma, J., Kim, J., Kirkby, J.,  
981 Kupc, A., Lehtipalo, K., Leiminger, M., Makhmutov, V., Onnela, A., Ortega, I. K., Petäjä, T., Praplan,

- 982 A. P., Riccobono, F., Rissanen, M. P., Rondo, L., Schnitzhofer, R., Schobesberger, S., Smith, J. N.,  
983 Steiner, G., Stozhkov, Y., Tomé, A., Tröstl, J., Tsagkogeorgas, G., Wagner, P. E., Wimmer, D., Ye,  
984 P., Baltensperger, U., Carslaw, K., Kulmala, M., and Curtius, J.: Experimental particle formation rates  
985 spanning tropospheric sulfuric acid and ammonia abundances, ion production rates, and temperatures,  
986 *J. Geophys. Res.*, 121, 12,377-312,400, 10.1002/2015jd023908, 2016.
- 987 Lee, S.-H., et al., New particle formation observed in the tropical/subtropical cirrus clouds, *J. Geophys. Res.*,  
988 109, D20209, doi:10.1029/2004JD005033, 2004.
- 989 Lovejoy, E. R., Curtius, J., and Froyd, K. D.: Atmospheric ion-induced nucleation of sulfuric acid and water,  
990 *J. Geophys. Res.*, 109, 10.1029/2003jd004460, 2004.
- 991 Merikanto, J., Napari, I., Vehkamäki, H., Anttila, T., and Kulmala, M.: New parameterization of sulfuric acid-  
992 ammonia-water ternary nucleation rates at tropospheric conditions, *J. Geophys. Res.*, 112,  
993 10.1029/2006jd007977, 2007.
- 994 Metzger, A., Verheggen, B., Dommen, J., Duplissy, J., Prevot, A. S. H., Weingartner, E., Riipinen, I., Kulmala,  
995 M., Spracklen, D. V., Carslaw, K. S., and Baltensperger, U.: Evidence for the role of organics in  
996 aerosol particle formation under atmospheric conditions, *Proc. Natl. Acad. Sci.*, 107, 6646-6651,  
997 10.1073/pnas.0911330107, 2010.
- 998 Murphy, D. M., Cziczo, D. J., Froyd, K. D., Hudson, P. K., Matthew, B. M., Middlebrook, A. M., Peltier, R.  
999 E., Sullivan, A., Thomson, D. S., and Weber, R. J.: Single-particle mass spectrometry of tropospheric  
1000 aerosol particles, *J. Geophys. Res.*, 111, 10.1029/2006jd007340, 2006.
- 1001 Napari, I., Noppel, M., Vehkamäki, H., and Kulmala, M.: Parametrization of ternary nucleation rates for  
1002  $\text{H}_2\text{SO}_4\text{-NH}_3\text{-H}_2\text{O}$  vapors, *J. Geophys. Res.*, 107, AAC 6-1-AAC 6-6, 10.1029/2002jd002132, 2002.
- 1003 NASA Langley <https://www-pm.larc.nasa.gov/> last accessed on June 1, 2018.
- 1004 National Centers for Environmental Prediction, Nation Weather Service, NOAA, U.S. Department of  
1005 Commerce. NCEP GFS 0.25 degree global forecast grids historical archive. Research Data Archive  
1006 at the National Center for Atmospheric Research, Computational and Information Systems  
1007 Laboratory. Doi.org/10.5065/D65D8PWK. Accessed 28 May 2018 (2015, updated daily).
- 1008 Perry, K. D., and P. V. Hobbs, Further evidence for particle nucleation in clear air adjacent to marine cumulus  
1009 clouds, *J. Geophys. Res.*, 99, 22,803–22,818, doi:10.1029/94JD01926, 1994.
- 1010 Pierce, J. R., and Adams, P. J.: Efficiency of cloud condensation nuclei formation from ultrafine particles,  
1011 *Atmos. Chem. Phys.*, 7, 1367-1379, 10.5194/acp-7-1367-2007, 2007.
- 1012 Pierce, J. R., and Adams, P. J.: Can cosmic rays affect cloud condensation nuclei by altering new particle  
1013 formation rates?, *Geophys. Res. Lett.*, 36, 10.1029/2009gl037946, 2009.
- 1014 Pierce, J. R., Riipinen, I., Kulmala, M., Ehn, M., Petäjä, T., Junninen, H., Worsnop, D. R., and Donahue, N.  
1015 M.: Quantification of the volatility of secondary organic compounds in ultrafine particles during  
1016 nucleation events, *Atmos. Chem. Phys.*, 11, 9019-9036, 10.5194/acp-11-9019-2011, 2011.
- 1017 Pierce, J. R.: Cosmic rays, aerosols, clouds, and climate: Recent findings from the CLOUD experiment, *J.*  
1018 *Geophys. Res.*, 122, 8051-8055, 10.1002/2017jd027475, 2017.
- 1019 Quinn, P. K., Bates, T. S., Coffman, D. J., and Covert, D. S.: Influence of particle size and chemistry on the  
1020 cloud nucleating properties of aerosols, *Atmos. Chem. Phys.*, 8, 1029-1042, 10.5194/acp-8-1029-  
1021 2008, 2008.
- 1022 Quinn, P. K., Coffman, D. J., Johnson, J. E., Upchurch, L. M., and Bates, T. S.: Small fraction of marine cloud  
1023 condensation nuclei made up of sea spray aerosol, *Nature Geosci.*, 10, 674, 10.1038/ngeo3003, 2017.
- 1024 Raes, F.: Entrainment of free tropospheric aerosols as a regulating mechanism for cloud condensation nuclei  
1025 in the remote marine boundary layer, *J. Geophys. Res.*, 100, 2893-2903, 10.1029/94jd02832, 1995.
- 1026 Raes, F., Van Dingenen, R., Cuevas, E., Van Velthoven, P. F. J., and Prospero, J. M.: Observations of aerosols  
1027 in the free troposphere and marine boundary layer of the subtropical Northeast Atlantic: Discussion

1028 of processes determining their size distribution, *J. Geophys. Res.*, 102, 21315-21328,  
1029 10.1029/97jd01122, 1997.

1030 Riccobono, F., Schobesberger, S., Scott, C. E., Dommen, J., Ortega, I. K., Rondo, L., Almeida, J., Amorim,  
1031 A., Bianchi, F., Breitenlechner, M., David, A., Downard, A., Dunne, E. M., Duplissy, J., Ehrhart, S.,  
1032 Flagan, R. C., Franchin, A., Hansel, A., Junninen, H., Kajos, M., Keskinen, H., Kupc, A., Kürten, A.,  
1033 Kvashin, A. N., Laaksonen, A., Lehtipalo, K., Makhmutov, V., Mathot, S., Nieminen, T., Onnela, A.,  
1034 Petäjä, T., Praplan, A. P., Santos, F. D., Schallhart, S., Seinfeld, J. H., Sipilä, M., Spracklen, D. V.,  
1035 Stozhkov, Y., Stratmann, F., Tomé, A., Tsagkogeorgas, G., Vaattovaara, P., Viisanen, Y., Vrtala, A.,  
1036 Wagner, P. E., Weingartner, E., Wex, H., Wimmer, D., Carslaw, K. S., Curtius, J., Donahue, N. M.,  
1037 Kirkby, J., Kulmala, M., Worsnop, D. R., and Baltensperger, U.: Oxidation products of biogenic  
1038 emissions contribute to nucleation of atmospheric particles, *Science*, 344, 717-721,  
1039 10.1126/science.1243527, 2014.

1040 Riipinen, I., Sihto, S. L., Kulmala, M., Arnold, F., Dal Maso, M., Birmili, W., Saarnio, K., Teinilä, K.,  
1041 Kerminen, V. M., Laaksonen, A., and Lehtinen, K. E. J.: Connections between atmospheric sulphuric  
1042 acid and new particle formation during QUEST III-IV campaigns in Heidelberg and Hyytiälä, *Atmos.*  
1043 *Chem. Phys.*, 7, 1899-1914, 10.5194/acp-7-1899-2007, 2007.

1044 Riipinen, I., Pierce, J. R., Yli-Juuti, T., Nieminen, T., Häkkinen, S., Ehn, M., Junninen, H., Lehtipalo, K.,  
1045 Petäjä, T., Slowik, J., Chang, R., Shantz, N. C., Abbatt, J., Leaitch, W. R., Kerminen, V. M., Worsnop,  
1046 D. R., Pandis, S. N., Donahue, N. M., and Kulmala, M.: Organic condensation: a vital link connecting  
1047 aerosol formation to cloud condensation nuclei (CCN) concentrations, *Atmos. Chem. Phys.*, 11, 3865-  
1048 3878, 10.5194/acp-11-3865-2011, 2011.

1049 Rollins, A. W., Thornberry, T. D., Ciciora, S. J., McLaughlin, R. J., Watts, L. A., Hanisco, T. F., Baumann,  
1050 E., Giorgetta, F. R., Bui, T. V., Fahey, D. W., and Gao, R. S.: A laser-induced fluorescence instrument  
1051 for aircraft measurements of sulfur dioxide in the upper troposphere and lower stratosphere, *Atmos.*  
1052 *Meas. Tech.*, 9, 4601-4613, 10.5194/amt-9-4601-2016, 2016.

1053 Rollins, A. W., Thornberry, T. D., Watts, L. A., Yu, P., Rosenlof, K. H., Mills, M., Baumann, E., Giorgetta,  
1054 F. R., Bui, T. V., Höpfner, M., Walker, K. A., Boone, C., Bernath, P. F., Colarco, P. R., Newman, P.  
1055 A., Fahey, D. W., and Gao, R. S.: The role of sulfur dioxide in stratospheric aerosol formation  
1056 evaluated by using in situ measurements in the tropical lower stratosphere, *Geophys. Res. Lett.*, 44,  
1057 4280-4286, 10.1002/2017gl072754, 2017.

1058 Rollins, A. W., Thornberry, T. D., Atlas, E., Navarro, M., Schauffler, S., Moore, F., Elkins, J. W., Ray, E.,  
1059 Rosenlof, K., Aquila, V., and Gao, R.-S.: SO<sub>2</sub> Observations and Sources in the Western Pacific  
1060 Tropical Tropopause Region, *J. Geophys. Res.*, 123, 13,549-513,559, 10.1029/2018jd029635, 2018.

1061 Scott, S. G., Bui, T. P., Chan, K. R., and Bowen, S. W.: The meteorological measurement system on the NASA  
1062 ER-2 aircraft, *J. Atmos. Ocean. Technol.*, 7, 525-540, 10.1175/1520-  
1063 0426(1990)007<0525:Tmmsot>2.0.Co;2, 1990.

1064 Seinfeld, J. H., and Pandis, S. N.: *Atmospheric Chemistry and Physics: From Air Pollution to Climate Change*,  
1065 Wiley, 2006.

1066 Sihto, S. L., Kulmala, M., Kerminen, V. M., Dal Maso, M., Petäjä, T., Riipinen, I., Korhonen, H., Arnold, F.,  
1067 Janson, R., Boy, M., Laaksonen, A., and Lehtinen, K. E. J.: Atmospheric sulphuric acid and aerosol  
1068 formation: implications from atmospheric measurements for nucleation and early growth  
1069 mechanisms, *Atmos. Chem. Phys.*, 6, 4079-4091, 10.5194/acp-6-4079-2006, 2006.

1070 Simon, M., Dada, L., Heinritzi, M., Scholz, W., Stolzenburg, D., Fischer, L., Wagner, A. C., Kürten, A.,  
1071 Rörup, B., He, X.-C., Almeida, J., Baalbaki, R., Baccarini, A., Bauer, P. S., Beck, L., Bergen, A.,  
1072 Bianchi, F., Bräkling, S., Brilke, S., Caudillo, L., Chen, D., Chu, B., Dias, A., Draper, D. C., Duplissy,  
1073 J., El Haddad, I., Finkenzeller, H., Frege, C., Gonzalez-Carracedo, L., Gordon, H., Granzin, M.,

1074 Hakala, J., Hofbauer, V., Hoyle, C. R., Kim, C., Kong, W., Lamkaddam, H., Lee, C. P., Lehtipalo, K.,  
1075 Leiminger, M., Mai, H., Manninen, H. E., Marie, G., Marten, R., Mentler, B., Molteni, U., Nichman,  
1076 L., Nie, W., Ojdanic, A., Onnela, A., Partoll, E., Petäjä, T., Pfeifer, J., Philippov, M., Quéléver, L. L.  
1077 J., Ranjithkumar, A., Rissanen, M., Schallhart, S., Schobesberger, S., Schuchmann, S., Shen, J., Sipilä,  
1078 M., Steiner, G., Stozhkov, Y., Tauber, C., Tham, Y. J., Tomé, A. R., Vazquez-Pufleau, M., Vogel, A.,  
1079 Wagner, R., Wang, M., Wang, D. S., Wang, Y., Weber, S. K., Wu, Y., Xiao, M., Yan, C., Ye, P., Ye,  
1080 Q., Zauner-Wieczorek, M., Zhou, X., Baltensperger, U., Dommen, J., Flagan, R. C., Hansel, A.,  
1081 Kulmala, M., Volkamer, R., Winkler, P. M., Worsnop, D. R., Donahue, N. M., Kirkby, J., and Curtius,  
1082 J.: Molecular understanding of new-particle formation from alpha-pinene between  $-50^{\circ}\text{C}$  and  $25^{\circ}\text{C}$ ,  
1083 *Atmos. Chem. Phys. Discuss.*, <https://doi.org/10.5194/acp-2019-1058>, in review, 2020.

1084 Smith, J.N.; Moore, K.F.; McMurry, P.H.; Eisele, F.L. Atmospheric Measurements of Sub-20 nm Diameter  
1085 Particle Chemical Composition by Thermal Desorption Chemical Ionization Mass Spectrometry.  
1086 *Aerosol Sci. Technol.*, 38, 100–110, 2004

1087 Stevens, B., G. Feingold, W. R. Cotton, and R. L. Walko, 1996: Elements of the microphysical structure of  
1088 numerically simulated nonprecipitating stratocumulus. *J. Atmos. Sci.*, 53, 980–1006,  
1089 [https://doi.org/10.1175/1520-0469\(1996\)053<0980:EOTMSO>2.0.CO;2](https://doi.org/10.1175/1520-0469(1996)053<0980:EOTMSO>2.0.CO;2).

1090 Ström, J., H. Fischer, J. Lelieveld, and F. Schröder, In situ measurements of microphysical properties and trace  
1091 gases in two cumulonimbus anvils over western Europe, *J. Geophys. Res.*, 104, 12,221 – 12,226, 1999.

1092 Thornton, D. C., Bandy, A. R., Blomquist, B. W., Talbot, R. W., and Dibb, J. E.: Transport of sulfur dioxide  
1093 from the Asian Pacific Rim to the North Pacific troposphere, *J. Geophys. Res.*, 102, 28489-28499,  
1094 10.1029/97jd01818, 1997.

1095 Twohy, C. H., Clement, C. F., Gandrud, B. W., Weinheimer, A. J., Campos, T. L., Baumgardner, D., Brune,  
1096 W. H., Faloon, I., Sachse, G. W., Vay, S. A., and Tan, D.: Deep convection as a source of new  
1097 particles in the midlatitude upper troposphere, *J. Geophys. Res.*, 107, AAC 6-1-AAC 6-10,  
1098 10.1029/2001jd000323, 2002.

1099 Twomey, S.: Pollution and the planetary albedo, *Atmos. Environ.*, 8, 1251-1256,  
1100 [https://doi.org/10.1016/0004-6981\(74\)90004-3](https://doi.org/10.1016/0004-6981(74)90004-3), 1974.

1101 Vehkamäki, H., Kulmala, M., Napari, I., Lehtinen, K. E. J., Timmreck, C., Noppel, M., and Laaksonen, A.:  
1102 An improved parameterization for sulfuric acid–water nucleation rates for tropospheric and  
1103 stratospheric conditions, *J. Geophys. Res.*, 107, AAC 3-1-AAC 3-10, 10.1029/2002jd002184, 2002.

1104 Veres PR, Neuman JA, Bertram TH, et al. Global airborne sampling reveals a previously unobserved dimethyl  
1105 sulfide oxidation mechanism in the marine atmosphere. *Proc Natl Acad Sci U S A.*; 117(9):4505-  
1106 4510. doi:10.1073/pnas.1919344117, 2020.

1107 Waddicor, D. A., Vaughan, G., Choulaton, T. W., Bower, K. N., Coe, H., Gallagher, M., Williams, P. I.,  
1108 Flynn, M., Volz-Thomas, A., Pätz, H.-W., Isaac, P., Hacker, J., Arnold, F., Schlager, H., and  
1109 Whiteway, J. A.: Aerosol observations and growth rates downwind of the anvil of a deep tropical  
1110 thunderstorm, *Atmos. Chem. Phys.*, 12, 6157–6172, <https://doi.org/10.5194/acp-12-6157-2012>, 2012.

1111 Weber, R., McMurry, P. H., Eisele, F., and Tanner, D.: Measurement of expected nucleation precursor species  
1112 and 3–500-nm diameter particles at Mauna Loa observatory, Hawaii, *J. of Atmos. Sci.*, 2242–2257,  
1113 1995.

1114 Weber, R. J., Marti, J. J., McMurry, P. H., Eisele, F. L., Tanner, D. J., and Jefferson, A.: Measurements of  
1115 new particle formation and ultrafine particle growth rates at a clean continental site, *J. Geophys. Res.*,  
1116 102, 4375–4385, 10.1029/96jd03656, 1997.

1117 Weber, R. J., Clarke, A. D., Litchy, M., Li, J., Kok, G., Schillawski, R. D., and McMurry, P. H.: Spurious  
1118 aerosol measurements when sampling from aircraft in the vicinity of clouds, *J. Geophys. Res.*, 103,  
1119 28337-28346, 10.1029/98jd02086, 1998.

- 1120 Weigel, R., Borrmann, S., Kazil, J., Minikin, A., Stohl, A., Wilson, J. C., Reeves, J. M., Kunkel, D., de Reus,  
1121 M., Frey, W., Lovejoy, E. R., Volk, C. M., Viciani, S., D'Amato, F., Schiller, C., Peter, T., Schlager,  
1122 H., Cairo, F., Law, K. S., Shur, G. N., Belyaev, G. V., and Curtius, J.: In situ observations of new  
1123 particle formation in the tropical upper troposphere: the role of clouds and the nucleation mechanism,  
1124 *Atmos. Chem. Phys.*, 11, 9983-10010, 10.5194/acp-11-9983-2011, 2011.
- 1125 Weigelt, A., Hermann, M., van Velthoven, P. F. J Brennkmeijer, C. A. M., Schlaf, G. and co-authors.  
1126 Influence of clouds on aerosol particle number concentrations in the upper troposphere. *J. Geophys.*  
1127 *Res.* 114, D01204, doi:10.01210.01029/02008JD009805, 2009.
- 1128 Westervelt, D. M., Pierce, J. R., Riipinen, I., Trivitayanurak, W., Hamed, A., Kulmala, M., Laaksonen, A.,  
1129 Decesari, S., and Adams, P. J.: Formation and growth of nucleated particles into cloud condensation  
1130 nuclei: model-measurement comparison, *Atmos. Chem. Phys.*, 13, 7645-7663, 10.5194/acp-13-7645-  
1131 2013, 2013.
- 1132 Westervelt, D. M., Pierce, J. R., and Adams, P. J.: Analysis of feedbacks between nucleation rate, survival  
1133 probability and cloud condensation nuclei formation, *Atmos. Chem. Phys.*, 14, 5577-5597,  
1134 10.5194/acp-14-5577-2014, 2014.
- 1135 Williamson, C., Kupc, A., Wilson, J., Gesler, D. W., Reeves, J. M., Erdesz, F., McLaughlin, R., and Brock,  
1136 C. A.: Fast time response measurements of particle size distributions in the 3–60 nm size range with  
1137 the nucleation mode aerosol size spectrometer, *Atmos. Meas. Tech.*, 11, 3491-3509, 10.5194/amt-11-  
1138 3491-2018, 2018.
- 1139 Williamson, C. J., Kupc, A., Axisa, D., Bilsback, K. R., Bui, T., Campuzano-Jost, P., Dollner, M., Froyd, K.  
1140 D., Hodshire, A. L., Jimenez, J. L., Kodros, J. K., Luo, G., Murphy, D. M., Nault, B. A., Ray, E. A.,  
1141 Weinzierl, B., Wilson, J. C., Yu, F., Yu, P., Pierce, J. R., and Brock, C. A.: A large source of cloud  
1142 condensation nuclei from new particle formation in the tropics, *Nature*, 574, 399-403,  
1143 10.1038/s41586-019-1638-9, 2019.
- 1144 Willis, M. D., Burkart, J., Thomas, J. L., Köllner, F., Schneider, J., Bozem, H., Hoor, P. M., Aliabadi, A. A.,  
1145 Schulz, H., Herber, A. B., Leaitch, W. R., and Abbatt, J. P. D.: Growth of nucleation mode particles  
1146 in the summertime Arctic: a case study, *Atmos. Chem. Phys.*, 16, 7663-7679, 10.5194/acp-16-7663-  
1147 2016, 2016.
- 1148 Wofsy, S.C., S. Afshar, H.M. Allen, E.C. Apel, E.C. Asher, B. Barletta, J. Bent, H. Bian, B.C. Biggs, D.R.  
1149 Blake, N. Blake, I. Bourgeois, C.A. Brock, W.H. Brune, J.W. Budney, T.P. Bui, A. Butler, P.  
1150 Campuzano-Jost, C.S. Chang, M. Chin, R. Commane, G. Correa, J.D. Crouse, P. D. Cullis, B.C.  
1151 Daube, D.A. Day, J.M. Dean-Day, J.E. Dibb, J.P. DiGangi, G.S. Diskin, M. Dollner, J.W. Elkins, F.  
1152 Erdesz, A.M. Fiore, C.M. Flynn, K.D. Froyd, D.W. Gesler, S.R. Hall, T.F. Hanisco, R.A. Hannun,  
1153 A.J. Hills, E.J. Hints, A. Hoffman, R.S. Hornbrook, L.G. Huey, S. Hughes, J.L. Jimenez, B.J.  
1154 Johnson, J.M. Katich, R.F. Keeling, M.J. Kim, A. Kupc, L.R. Lait, J.-F. Lamarque, J. Liu, K. McKain,  
1155 R.J. Mclaughlin, S. Meinardi, D.O. Miller, S.A. Montzka, F.L. Moore, E.J. Morgan, D.M. Murphy,  
1156 L.T. Murray, B.A. Nault, J.A. Neuman, P.A. Newman, J.M. Nicely, X. Pan, W. Paplawsky, J. Peischl,  
1157 M.J. Prather, D.J. Price, E. Ray, J.M. Reeves, M. Richardson, A.W. Rollins, K.H. Rosenlof, T.B.  
1158 Ryerson, E. Scheuer, G.P. Schill, J.C. Schroder, J.P. Schwarz, J.M. St.Clair, S.D. Steenrod, B.B.  
1159 Stephens, S.A. Strode, C. Sweeney, D. Tanner, A.P. Teng, A.B. Thames, C.R. Thompson, K.  
1160 Ullmann, P.R. Veres, N. Vieznor, N.L. Wagner, A. Watt, R. Weber, B. Weinzierl, P.O. Wennberg,  
1161 C.J. Williamson, J.C. Wilson, G.M. Wolfe, C.T. Woods, and L.H. Zeng. 2018. ATom: Merged  
1162 atmospheric chemistry, trace gases, and aerosols. ORNL DAAC, Oak Ridge, Tennessee, USA.  
1163 <https://doi.org/10.3334/ORNLDAAC/1581>
- 1164 Yu, F., Luo, G., Bates, T. S., Anderson, B., Clarke, A., Kapustin, V., Yantosca, R. M., Wang, Y., and Wu, S.:  
1165 Spatial distributions of particle number concentrations in the global troposphere: Simulations,

1166 observations, and implications for nucleation mechanisms, *J. Geophys. Res.*, 115,  
1167 10.1029/2009jd013473, 2010.

1168 Yu, F.: Ion-mediated nucleation in the atmosphere: Key controlling parameters, implications, and look-up  
1169 table, *J. Geophys. Res.*, 115, D03206, doi:10.1029/2009JD012630, 2010.

1170 Yu, F., Luo, G., Nadykto, A. B., and Herb, J.: Impact of temperature dependence on the possible contribution  
1171 of organics to new particle formation in the atmosphere, *Atmos. Chem. Phys.*, 17, 4997-5005,  
1172 10.5194/acp-17-4997-2017, 2017.

1173 Yu, F., Nadykto, A. B., Luo, G., and Herb, J.: H<sub>2</sub>SO<sub>4</sub>-H<sub>2</sub>O binary and H<sub>2</sub>SO<sub>4</sub>-H<sub>2</sub>O-NH<sub>3</sub> ternary  
1174 homogeneous and ion-mediated nucleation: lookup tables version 1.0 for 3-D modeling application,  
1175 *Geosci. Model Dev.*, 13, 2663-2670, <https://doi.org/10.5194/gmd-13-2663-2020>, 2020.

1176 Yue, G. K., and Hamill, P.: The homogeneous nucleation rates of H<sub>2</sub>SO<sub>4</sub>-H<sub>2</sub>O aerosol particles in air, *Journal*  
1177 *of Aerosol Science*, 10, 609-614, [https://doi.org/10.1016/0021-8502\(79\)90023-5](https://doi.org/10.1016/0021-8502(79)90023-5), 1979.

1178 Zhang, Y., McMurry, P. H., Yu, F., and Jacobson, M. Z.: A comparative study of nucleation parameterizations:  
1179 1. Examination and evaluation of the formulations, *J. Geophys. Res.*, 115, 10.1029/2010jd014150,  
1180 2010.

1181 Zhu, J., Penner, J. E., Yu, F., Sillman, S., Andreae, M. O. and Coe, H.: Decrease in radiative forcing by organic  
1182 aerosol nucleation, climate, and land use change, *Nat. Commun.*, 10(1), doi:10.1038/s41467-019-  
1183 08407-7, 2019.